Abdominal Radiology (2022) 47:1473–1502
https://doi.org/10.1007/s00261-022-03462-z

REVIEW

Imaging findings of spontaneous intraabdominal hemorrhage: neoplastic and non-neoplastic causes

Sevtap Arslan[1] · Yasin Sarıkaya[2] · Deniz Akata[3] · Mustafa Nasuh Özmen[3] · Muşturay Karçaaltıncaba[3] · Ali Devrim Karaosmanoğlu[3]

Received: 10 January 2022 / Revised: 14 February 2022 / Accepted: 16 February 2022 / Published online: 1 March 2022

Abstract

Contrary to traumatic and iatrogenic intraabdominal hemorrhages, spontaneous intraabdominal hemorrhage is a challenging clinical situation. A variety of neoplastic and non-neoplastic conditions may cause spontaneous intraabdominal bleeding. Imaging findings vary depending on the source of bleeding and the underlying cause. In this article, we aim to increase the awareness of imagers to the most common causes of spontaneous intraabdominal hemorrhage by using representative cases.

Keywords Abdominal cavity · Adrenal gland neoplasms · Hemorrhage · Gastrointestinal tract · Gynecologic neoplasms · Kidney neoplasms · Liver neoplasms · Pancreas neoplasms · Retroperitoneal space · Spleen neoplasms

Introduction

Spontaneous intraabdominal hemorrhage due to neoplastic and non-neoplastic diseases is a challenging clinical situation as majority of the cases present with nonspecific symptoms, such as abdominal pain, hypotension, vomiting, and malaise. In rare cases, spontaneous intraabdominal bleeding may be the presenting manifestation. As the symptoms are nonspecific, imaging plays a crucial role in diagnosing and triaging these patients. However, detection of the source of hemorrhage may be challenging in imaging studies due to massive hemoperitoneum. Nevertheless, some imaging findings may indicate the anatomic site of hemorrhage, such as 'sentinel clot' sign on computed tomography (CT). Sentinel clot sign is described as the highest attenuation hematoma adjacent to the bleeding organ. Furthermore, the underlying cause of hemorrhage (neoplasms or non-neoplastic diseases) may not be accurately detected in the initial stage. The detection and diagnosis of a causative tumor may not be evident in imaging studies due to the large hematoma [1, 2]. As prompt and proper imaging plays such a fundamental role in clinical management, we aimed to review the expected imaging findings of these patients in this article. We also made a detailed literature search to summarize the radiological findings of these cases (Tables 1, 2) [3–73].

✉ Ali Devrim Karaosmanoğlu
alidevrim76@yahoo.com

Sevtap Arslan
sevtap.arsln@gmail.com

Yasin Sarıkaya
yasinsarikaya@hotmail.com.tr

Deniz Akata
akataden@gmail.com

Mustafa Nasuh Özmen
mozmen@hacettepe.edu.tr

Muşturay Karçaaltıncaba
musturayk@yahoo.com

[1] Department of Radiology, Suhut State Hospital, 03800 Afyon, Turkey

[2] Department of Radiology, Afyonkarahisar Health Sciences University, 03217 Afyon, Turkey

[3] Department of Radiology, Hacettepe University School of Medicine, Sihhiye, 06230 Ankara, Turkey

Liver

Neoplastic bleeding

Hepatocellular carcinoma

Hepatocellular carcinoma (HCC) is the third leading cause of overall cancer mortality and is among leading causes of death in patients with cirrhosis. Its morbidity and mortality are relentlessly increasing due to increased

Table 1 Spontaneously bleeding intraabdominal neoplasms

Origin of bleeding	Neoplasm	Associated imaging findings of lesions	Associated imaging findings of acute hemorrhage
Liver [3–28]*	HCC	– Arterial hyperenhancing mass demonstrating washout on portal venous and delayed phases – Intratumoral fat or hemorrhage	– Intratumoral hemorrhage • US: heterogeneous mass, multilaminated or whorled appearance, anechoic cystic areas, hyperechoic retracted clot • CT: hyperattenuating areas and fluid–fluid level on unenhanced phase • MRI: hyperintense areas on T1W images, hypointense areas or fluid–fluid level on T2W images, low ADC values in acute phase – Rupture • Focal discontinuity of the capsule around the tumor • Subcapsular liver hematoma • Hemoperitoneum • Peritoneal nodules from tumor spillage • Contrast media extravasation on CTA in active bleeding
	Hemangioma	– Mostly hyperechoic on US – Discontinuous, peripheral, nodular enhancement on arterial phase – Progressive centripedal filling on portal and delayed phases	
	FNH	– Arterial hyperenhancing mass becoming isodense or isointense on portal and delayed phases – Isointense or hyperintense on HBP – Hyperintense central scar on T2W images, which may enhance on delayed phase	
	Metastases	– Usually hypovascular masses – NET, RCC, thyroid carcinoma, breast carcinoma, melanoma, and sarcoma metastases may be hypervascular	
	Adenoma	– Arterial hyperenhancing mass becoming isointense on portal and delayed phases – Delayed-enhancing pseudocapsule – Hypointense on HBP – T2-hyperintense band in inflammatory subtype – Intratumoral fat or hemorrhage	
	Hepatoblastoma	– Heterogeneously enhancing large mass in a pediatric patient – Intratumoral hemorrhage or calcification	
	Hepatic angiosarcoma	– Hemorrhagic, hypoattenuating heterogeneous mass	
Pancreas [30–35]*	Serous cystadenoma	– Most commonly located in head > > body or tail – Microcystic, macrocystic, or, solid in appearance – Central scar with calcifications – No communication with the pancreatic ductal system – Hyperenhancement is rare	– Intratumoral hemorrhage • Similar to findings detected in liver neoplasms – Rupture • A hemorrhagic pancreatic lesion with peripancreatic and perisplenic hematoma • Contrast media extravasation on CTA in active bleeding
	IPMN	– Location in the head > > body or tail – Communication with the pancreatic ductal system – Pancreatic duct dilatation – Enhancing solid component in malignant transformation	
	Mucinous cystadenoma	– Location in the tail or body – Macrocystic with thick septations – Peripheral calcifications – No communication with the pancreatic duct	
	NET	– Hyperenhancing mass – Rarely, cystic, or necrotic changes and calcification	

Table 1 (continued)

Origin of bleeding	Neoplasm	Associated imaging findings of lesions	Associated imaging findings of acute hemorrhage
Spleen [39–41]*	Angiosarcoma	– Hypervascular mass with necrosis and hemorrhage – Liver metastases may be present	– Intratumoral hemorrhage • Similar to findings detected in liver neoplasms – Rupture • Perisplenic hematoma • Hemoperitoneum • Peritoneal nodules from tumor spillage • Contrast media extravasation on CTA in active bleeding
Kidney [46–50]*	RCC	– Clear cell subtype hypervascular, and other subtypes mostly hypovascular – Necrosis and hemorrhage are common in papillary and clear cell subtypes – Microscopic fat may be detected on chemical shift imaging in clear cell RCC – Central scar and spoke-wheel enhancement may be seen in chromophobe subtype – Papillary subtype is hypointense on T2W images – Renal vein thrombus, metastases may be present	– Intratumoral hemorrhage • Similar to findings detected in liver neoplasms – Hemorrhage into collecting system • Unenhanced CT: hyperdense content within the renal pelvis and the ureter – Rupture • Perirenal hematoma • Contrast media extravasation on CTA in active bleeding
	AML	– Macroscopic fat – Microscopic fat may be detected on chemical shift imaging in lipid-poor AMLs – Lipid-poor AML is hypointense on T2W images	
	Oncocytoma	– Hypervascular lesion with spoke-wheel enhancement – Central scar – Segmental enhancement inversion	
Bladder [57]*	TCC	– Focal thickening of the bladder wall or mass protruding into lumen – Extension into perivesical fat, invasion of the adjacent organs or pelvic wall – Abnormally enlarged abdominal lymph nodes, metastases	– Bladder hematoma in severe hematuria

Table 1 (continued)

Origin of bleeding	Neoplasm	Associated imaging findings of lesions	Associated imaging findings of acute hemorrhage
Adrenal [59, 60]*	Adenoma	– Density lower than 10 HU on unenhanced CT – > 60% absolute washout and > 40% relative washout on adrenal CT protocol – Signal drop in the out of phase imaging – Atypical features, including hemorrhage or calcification, may be present – If lesion > 4 cm in size, malignancy should be suspected	– Intratumoral hemorrhage • Similar to findings detected in liver neoplasms – Rupture • Retroperitoneal hematoma • Contrast media extravasation on CTA in active bleeding
	Neuroblastoma	– Heterogeneously enhancing mass with internal calcifications in a pediatric patient	
	ACC	– Heterogeneous, irregular mass with necrosis and calcifications – Usually > 6 cm in size – Tumor thrombus in the veins	
	Pheochromocytoma	– Avidly enhancing mass with internal cystic areas and calcifications – T2 hyperintensity	
	Lymphoma	– Infiltrative, heterogeneous mass – Bilateral involvement – Preserved adreniform shape of the glands	
	Metastases	– Contrast enhancing mass in patients with known malignancy	
GI tract [62]*	Adenocarcinoma[µ]	– Circumferential bowel wall thickening or mass protruding into lumen – Abnormally enlarged abdominal lymph nodes, liver metastases – Complications (intestinal obstruction or perforation) may be present	– GI bleeding • Intraluminal hyperdense content on unenhanced phase of CTA • Contrast media extravasation on arterial and venous phases in active bleeding
Gynecologic causes [66]*	Endometrial carcinoma	– Heterogeneous mass enhancing less than normal endometrium – Low ADC values on DWI – Invasion of adjacent organs	– Intraperitoneal bleeding – GI bleeding – Hematuria (The findings of the bleeding types mentioned above are specified in the relevant sections)
	Cervical cancer	– T2-hyperintense mass enhancing more than normal cervical stroma – Invasion of parametrium or adjacent organs	
Retroperitoneum [70]*	Neurofibroma	– Well-defined round-shaped homogeneous mass – Cystic areas from myxoid degeneration – Large size, extensively infiltrating, solid mass in patients with plexiform neurofibroma	– Intratumoral hemorrhage • Similar to findings detected in liver neoplasms – Rupture • Retroperitoneal hematoma • Contrast media extravasation on CTA in active bleeding
	Lymphoma	– Well-defined homogeneously enhancing mass encasing abdominal aorta and IVC without luminal compression – Calcification and necrosis may develop after chemotherapy	

ACC adrenocortical carcinoma, *ADC* apparent diffusion coefficient, *AML* angiomyolipoma, *CT* computed tomography, *CTA* CT angiography, *DWI* diffusion-weighted imaging, *FNH* focal nodular hyperplasia, *GI* gastrointestinal, *HBP* hepatobiliary phase, *HCC* hepatocellular carcinoma, *HU* Hounsfield unit, *IPMN* intraductal papillary mucinous neoplasm, *IVC* inferior vena cava, *MRI* magnetic resonance imaging, *NET* neuroendocrine tumor, *RCC* renal cell carcinoma, *T1W* T1-weighted, *T2W* T2-weighted, *TCC* transitional cell carcinoma, *US* ultrasonography

*References

[µ]Other GI tumors not mentioned here may also present with GI bleeding

Table 2 Non-neoplastic spontaneous intraabdominal bleeding

Origin of bleeding	Underlying cause	Associated imaging findings of disease	Associated imaging findings of acute hemorrhage
Liver [27–29]*	Hepatic cyst	– US: well-marginated anechoic lesion with thin wall, posterior acoustic enhancement – CT: homogeneous hypoattenuating lesion (< 10 HU), no enhancement after IV contrast – MRI: homogeneous low signal intensity on T1W images, high signal intensity on T2W images, no enhancement after IV contrast	– Intralesional hemorrhage • US: complex cystic lesion with thick mobile septae, fluid–fluid level, intracystic nodules (representing retracted clot), lack of internal vascularity • CT: hyperattenuating areas and fluid–fluid level on unenhanced images, non-enhancing septae or mural nodularity after IV contrast • MRI: hyperintense areas on T1W images, hypointense areas or fluid–fluid level on T2W images, non-enhancing septae or mural nodularity – Rupture • Subcapsular liver hematoma • Hemoperitoneum
	Cirrhosis	– Surface nodularity, segmental atrophy/hypertrophy – Regenerative, siderotic, or dysplastic nodules – Signs of portal hypertension	– Subcapsular liver hematoma – Hemoperitoneum – No detectable underlying neoplasm
Pancreas [30, 37, 38]*	Pseudocyst	– Irregularly marginated or well-circumscribed cystic lesion in patients with a history of acute pancreatitis – Dependent debris may be seen	– Intralesional hemorrhage • CT: hyperattenuating areas or fluid–fluid level on unenhanced phase • MRI: hyperintense areas on T1W images, hypointense areas or fluid–fluid level on T2W images – Rupture • Peripancreatic and/or perisplenic hematoma
	Endometrioma	– Thick-walled complex cyst with mural papillary nodules in premenopausal women	
	Pseudoaneurysm	– A well-marginated sac communicating with donor artery (mostly splenic or gastroduodenal artery)	– Rupture • Peripancreatic and/or perisplenic hematoma • Contrast media extravasation on CTA in active bleeding
Spleen [43–45]*	Epidermoid cyst	– US: anechoic lesion with low-level echoes – CT and MRI: follows the typical imaging characteristics of cysts elsewhere in the body, no enhancement after IV contrast	– Intralesional hemorrhage • Similar to findings detected in hemorrhagic liver cysts – Rupture • Perisplenic hematoma • Hemoperitoneum • Contrast media extravasation on CTA in active bleeding
	Sickle cell anemia	– Splenic infarcts	– Rupture • Perisplenic hematoma • Hemoperitoneum • Contrast media extravasation on CTA in active bleeding

Table 2 (continued)

Origin of bleeding	Underlying cause	Associated imaging findings of disease	Associated imaging findings of acute hemorrhage
Kidney [51–56]*	Renal cyst	– Similar to findings detected in liver cysts	– Intralesional hemorrhage • Similar to findings detected in hemorrhagic liver cysts – Rupture • Perirenal retroperitoneal hematoma
	Coagulopathy	– Hyperdense mural thickening of the renal pelvis and upper ureter – Central hyperdense mass adjacent to the renal pelvis – No enhancement	– Subepithelial hemorrhage
	Vasculitis	– Renal parenchyma may be normal – Renal infarcts and microaneurysms may be seen	– Perirenal retroperitoneal hematoma
Bladder [58]*	Coagulopathy	– Hyperdense lesion in the bladder lumen – Absence of enhancement and no obvious attachment to the bladder wall – Mobile on US	– Bladder hematoma
Adrenal [60, 61]*	– Coagulopathy – Metabolic stress – Antiphospholipid syndrome – Idiopathic	– Typical imaging findings of a hematoma – No underlying enhancing lesion	– Retroperitoneal hematoma
GI tract [63, 64]*	Angiodysplasia	– Areas of focal enhancement in the bowel wall – Early filling of an antimesenteric vein	– GI bleeding • Intraluminal hyperdense content on unenhanced phase of CTA • Contrast media extravasation on arterial and venous phases in active bleeding
	Coagulopathy	– Hyperdense mural thickening on unenhanced CT may suggest intramural hematoma	– GI bleeding – Intramural hematoma
	Pancreatitis (acute, chronic, or autoimmune)	– Hyperdense mural thickening on unenhanced CT	– Intramural duodenal hematoma
Gynecologic causes [67, 68]*	Ruptured ovarian cyst	– Cystic lesion with collapsed wall, low-level echoes and fine internal septations	– Hemoperitoneum
	Ruptured endometrioma	– Multilocular ovarian cyst with low-level echoes and hyperechoic wall foci – T2-hypointense, T1-hyperintense cyst on MRI – T2 shading and T2 dark spot sign – No enhancement	
	Ruptured ectopic pregnancy	– Tubal ring sign – Obvious live extrauterine pregnancy – Complex extra-adrenal mass with the typical "ring of fire" sign on color Doppler	

Table 2 (continued)

Origin of bleeding	Underlying cause	Associated imaging findings of disease	Associated imaging findings of acute hemorrhage
Retroperitoneum [72, 73]*	Coagulopathy	– A large hematoma with hematocrit level	– Retroperitoneal hematoma
	Vascular causes	– Intramural hematoma, increasing aneurysm size, "draped aorta" sign, "thrombus fissuration" sign may all indicate increased risk of rupture in AAA – Splanchnic aneurysms (mostly hepatic and splenic) may also rupture	

AAA abdominal aortic aneurysm, *CT* computed tomography, *CTA* CT angiography, *GI* gastrointestinal, *HBP* hepatobiliary phase, *HU* Hounsfield unit, *IV* intravenous, *MRI* magnetic resonance imaging, *T1W* T1-weighted, *T2W* T2-weighted, *US* ultrasonography

*References

rates of viral hepatitis and nonalcoholic steatohepatitis [4]. Radiological diagnosis of a typical HCC is relatively straightforward with multiphasic contrast-enhanced CT or magnetic resonance imaging (MRI). The Liver Imaging Reporting and Data System (LI-RADS), providing standardized terminology for imaging findings in liver lesions in patients at risk of HCC, suggests dividing lesions into five categories (LR 1–5) according to suspicious imaging findings. Major features of CT/MRI LI-RADS include non-rim arterial phase hyperenhancement, nonperipheral washout, enhancing capsule, size, and threshold growth. A typical HCC is scored as LR-5 and demonstrates non-rim arterial phase hyperenhancement with nonperipheral washout on portal venous and delayed phases [74]. On liver MRI studies using hepatocyte-specific contrast agent (gadoxetic acid), they mostly appear hypointense on hepatobiliary phase (HBP) images. In patients with these characteristic imaging features, the diagnosis of HCC may be firmly made in a noninvasive manner without any need for histopathologic confirmation [3, 4].

Despite the fact that spontaneous rupture of HCC is not common, it is a potentially life-threatening complication. It is the third leading cause of HCC-related death after tumor progression and liver failure. It is observed in 3–15% of patients, with a lower incidence reported in Western countries compared to Asian countries. The exact mechanism of spontaneous rupture is unclear and does not appear to correlate with tumor size. Spontaneous rupture appears to be more common in subcapsular tumors which are not fully covered by liver parenchyma [5, 6]. Intense tumor vascularity and parenchymal necrosis within the tumor, portal vein, or hepatic vein thrombosis are mentioned among inciting factors for spontaneous tumor rupture [7, 8]. The history of transarterial chemoembolization may also be counted among potential risk factors [9]. The clinical symptomatology appears to be related to the tumor location within liver parenchyma. Hemoperitoneum and hemodynamic instability are more common in peripherally located tumors, whereas rupture of the tumor deeply located within hepatic parenchyma may present with right upper quadrant pain or may even be asymptomatic [5–8]. CT is the imaging modality of choice in patients with hemodynamic instability when HCC rupture is suspected due to its wider availability and faster acquisition time. The detection of hemoperitoneum, perihepatic, or subcapsular hematoma, extravasation of contrast material, and focal discontinuity of the tumor capsule (enucleation sign) are suggestive imaging findings for tumor rupture (Fig. 1) [7, 8]. Emergent transarterial embolization of the tumor is the most common treatment approach in patients with active bleeding. Surgery may be considered in patients who are not responding to transarterial embolization [5, 6].

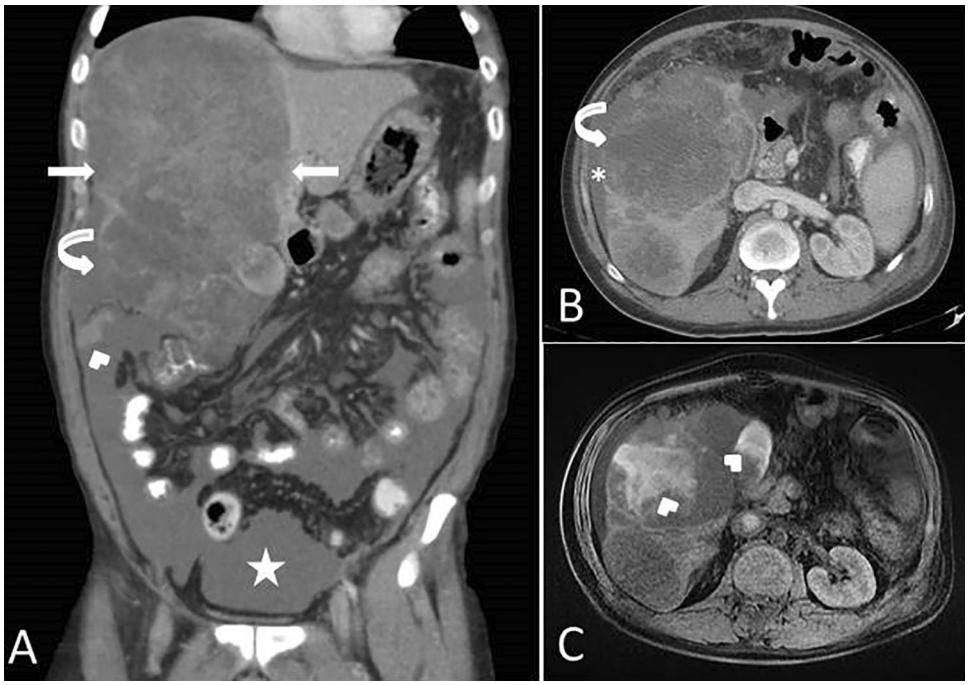

Fig. 1 40-year-old male patient with known HCC presents with right upper quadrant pain. **A** Coronal postcontrast CT image shows a large mass (arrows) almost completely replacing the right liver lobe. Focal discontinuity of the capsule (curved arrow), intraperitoneal clot (arrowhead), and pelvic fluid (star) suggest tumor rupture. **B** Axial postcontrast CT image demonstrates subcapsular hematoma (asterisk) and focal discontinuity of the capsule (curved arrow). **C** Axial precontrast T1W fat-saturated MR image shows internal hyperintensity of the mass suggestive intratumoral hemorrhage (arrowheads)

Hemangioma

Hemangiomas are the most common benign hepatic tumors with an estimated prevalence of 20% [10]. In the majority of the cases, hemangiomas are usually small sized (< 3 cm) and diagnosed incidentally. But, larger hemangiomas (> 4–5 cm), also known as cavernous or giant hemangiomas, may present nonspecific symptoms related to capsular distension, biliary obstruction, thrombosis, infarction, or gastric outlet obstruction. On imaging, hemangiomas are usually well-defined lesions. Hemangiomatosis, in which the boundary of the lesion is ill defined, is a rare condition characterized by diffuse replacement of liver parenchyma with hemangiomatous lesions. It usually occurs in infants and may present with palpable abdominal mass and high-output cardiac failure [10, 11].

Spontaneous rupture is an infrequent and potentially life-threatening complication of hemangioma with a high mortality rate of 35%. The risk of rupture is strongly correlated with size of the lesion and subcapsular location [10, 11]. Intratumoral bleeding is also rare. The interval enlargement of the lesion and increased echogenicity at ultrasound (US) are suggestive features for intratumoral bleeding. Increased density at unenhanced CT and high signal intensity at T1-weighted (T1W) MR images are other imaging features of intratumoral bleeding [12]. In case of rupture, hemoperitoneum and intraperitoneal clot formations are typically observed on imaging [11]. In these patients, the detection of a liver lesion with characteristic imaging features of a hemangioma is mostly diagnostic [10]. Conservative therapy, hepatic artery embolization, hepatic artery ligation, and resection are treatment options for hemorrhagic hemangioma [11].

Focal nodular hyperplasia

Focal nodular hyperplasia (FNH) is the most commonly detected benign liver mass after hemangioma and is reported to be found in 3% of the population, with a female predominance [12]. The vast majority of FNHs are incidentally detected small-sized lesions. Unlike hepatocellular adenoma (HCA), hemorrhage, and rupture are rarely seen in FNH with only anecdotal case reports [13]. In patients with hemorrhagic FNHs, the diagnosis may be challenging with imaging. MRI using hepatocyte-specific contrast agent is usually the preferred method for differentiating FNH from HCA and other liver tumors. Arterial phase postcontrast T1W images are critical for diagnosis as they may be hardly discernible on T2-weighted (T2W) and other pre- and postcontrast T1W images (Fig. 2). The presence of a so-called T2-hyperintense "central scar" is also another suggestive feature of FNH. The enhancement of this central area on the delayed phases of dynamic contrast-enhanced images is also helpful. HBP imaging is probably the most important phase for diagnosis. In this phase, FNHs appear isointense or hyperintense, as they contain mature hepatocytes, in contrast to HCAs, where they mostly appear hypointense [12, 14].

Hepatic metastases

Metastatic disease is the most common malignancy of the liver. The colon, breast, stomach, pancreas, and lung

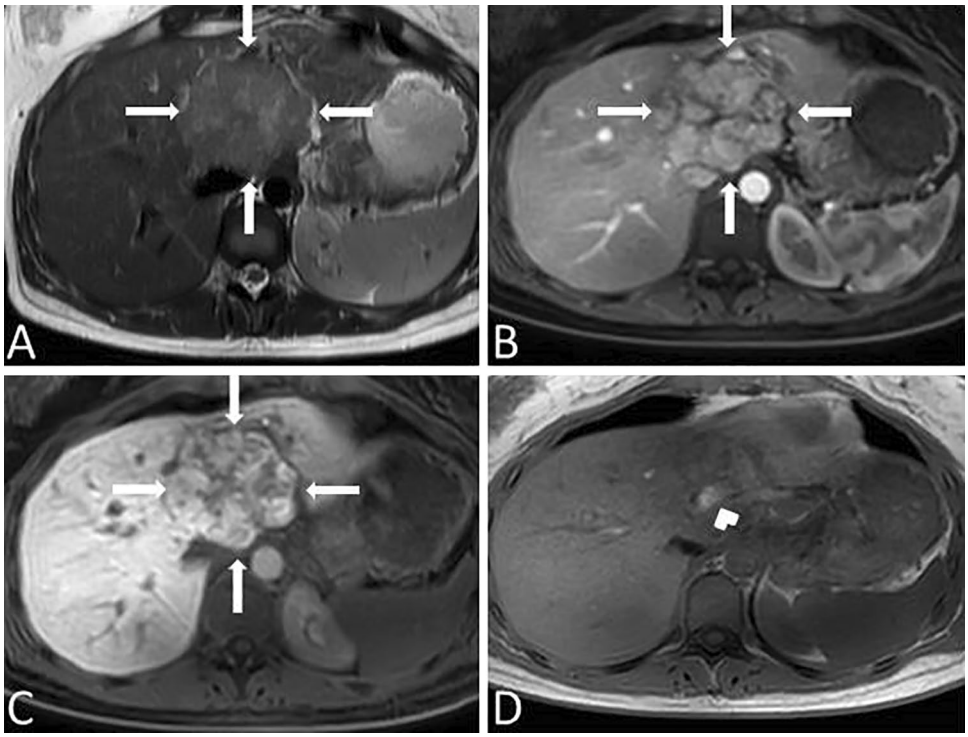

Fig. 2 37-year-old female patient with known breast cancer underwent abdominal MRI examination for staging. **A** Axial T2W MR image shows a heterogeneous mass (arrows) in the left liver lobe. **B** Post-contrast arterial phase T1W MR image demonstrates hypervascular nature of the mass (arrows). **C** The mass is isointense on the hepatobiliary phase (arrows). **D** Axial precontrast T1W image shows a hemorrhagic focus (arrowhead) within the lesion. Imaging findings were found to be consistent with FNH. Follow-up studies confirmed stability of this lesion

are the most common sources for liver metastases. While metastases are usually seen as multiple discrete lesions, they may also be observed as solitary lesions [15, 16]. In the imaging literature, metastases are broadly categorized as hypo- or hyperenhancing. Hyperenhancing liver metastases typically originate from neuroendocrine tumors (NETs), renal cell carcinoma (RCC), thyroid carcinoma, breast carcinoma, choriocarcinoma, melanoma, and sarcomas [12]. Hypoenhancing liver metastases are predominantly supplied by portal venous branches and, therefore, appear more conspicuous on portal venous phase images. In contrast, hyperenhancing metastases show significant contrast enhancement during the arterial phase due to their abundant arterial blood supply [14–16]. Both hypo- and hyperenhancing tumors have been reported to bleed spontaneously. There are no clear, established criteria outlining the risks of spontaneous bleeding in liver metastases [2, 12]. Metastases from lung tumors, RCCs, and melanomas are the most commonly reported types of liver metastases that spontaneously bleed [12]. Hemorrhagic metastases can demonstrate T1 hyperintensity on precontrast MR imaging (Fig. 3). However, this appearance should not be confused with metastases that have inherent T1 hyperintensity, such as metastases from melanomas (due to melanin content), colonic adenocarcinomas (due to coagulative necrosis), pancreatic mucinous cystadenocarcinomas (due to mucin), ovarian adenocarcinomas, and myelomas (due to protein) [15, 16]. Subcapsular hematomas may develop in patients with severe bleeding (Fig. 4) [12].

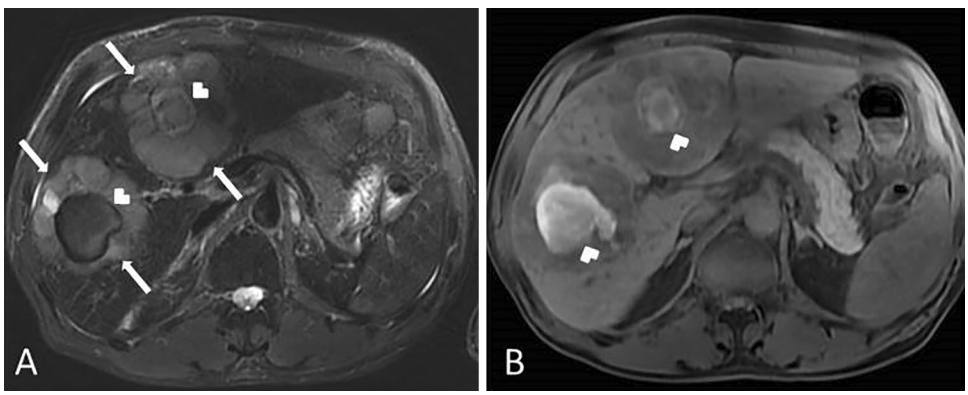

Fig. 3 54-year-old male patient with known metastatic small-bowel NET presents with right upper quadrant pain. **A** Axial T2W MR image shows large liver metastases (arrows) with T2-hypointense central zones (arrowheads), suggesting tumor hemorrhage. **B** Axial precontrast T1W MR image confirms the hemorrhagic components as hyperintense areas (arrowheads)

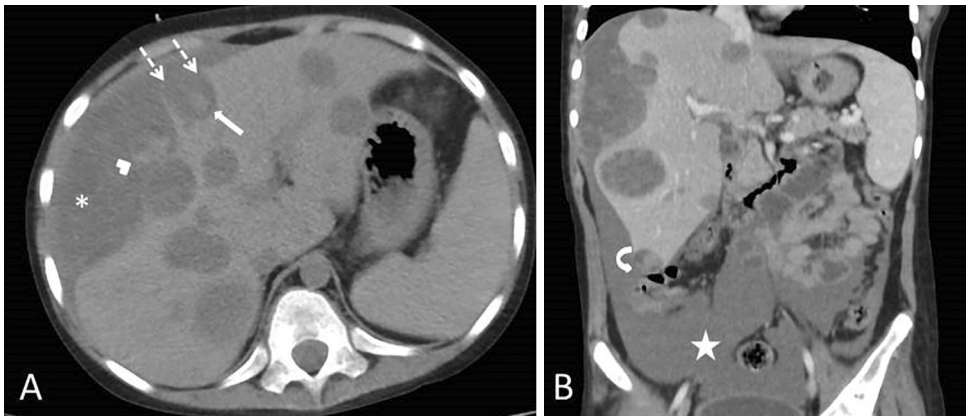

Fig. 4 30-year-old female patient with known synovial sarcoma presenting with acute abdominal pain. **A** Axial precontrast CT image shows multiple liver metastases. Focal discontinuity of the capsule (dashed arrows) around a subcapsular metastasis (arrow) and subcapsular liver hematoma (asterisk) with retracted clot (arrowhead) are suggestive of tumor rupture. **B** Coronal postcontrast CT image demonstrates another subcapsular metastasis with discontinuity of the capsule (curved arrow). Hemoperitoneum is also present (star). The patient died immediately after this scan

Adenoma

HCA is a rare liver tumor with an estimated incidence of 4/100.000 with a prominent female preponderance. It is reported to be associated with use of oral contraceptives and anabolic androgenic steroids, glycogen storage disease, diabetes mellitus, and iron overload secondary to chronic transfusion therapy. HCAs are commonly seen as solitary lesions, but they are multiple in around 20% of the patients [12]. The correct diagnosis of the HCA is critical because of the potential risk for malignant transformation and spontaneous hemorrhage [2, 12, 17]. Hemorrhage is a common complication of HCA and may be observed in 25% of the cases. Most hemorrhages are intratumoral; however, intraparenchymal and subcapsular hematomas or hemoperitoneum may also be observed. Large tumors greater than 5 cm in size, exophytic location, and inflammatory subtype are potential risk factors for spontaneous hemorrhage [17, 18].

On MRI, typical imaging findings of HCAs include arterial hypervascularity with a subsequent isointense appearance on portal venous and delayed phases. Enhancing tumor capsule may be seen in a subgroup of patients [14]. HCAs may show foci of T1 hyperintensity due to the presence of fat or blood products (Fig. 5). Fat-suppressed or opposed phase T1W MR images can differentiate fat from hemorrhage [14]. Acute intratumoral hemorrhage may be hyperechoic on US and hyperdense on unenhanced CT. Old hemorrhages appear hypoechoic or cystic on US and heterogeneous hypodense on CT [17].

Hepatoblastoma

Hepatoblastomas, which arise from hepatocyte precursors, constitute the majority of malignant liver masses in infancy and childhood [19]. US is generally the first imaging method in a child with suspected liver mass because of its wider accessibility and better patient cooperation. MRI is also frequently preferred due to its high soft-tissue resolution and lack of ionizing radiation. On MRI, a typical hepatoblastoma is T1-hypointense, T2 heterogeneous hyperintense, heterogeneously enhancing mass that may contain hemorrhage and calcification [20]. Despite being rare, tumor rupture has been reported and is considered a poor prognostic factor for progression-free survival. Ascites, peritoneal nodules, and subcapsular hematoma may give rise to suspicion for tumor rupture [21].

Hepatic angiosarcoma

Hepatic angiosarcoma (HA), albeit rare, is the most common malignant mesenchymal tumor of the liver and accounts for 2% of all primary liver tumors [22, 23]. Exposure to thorotrast, vinyl chloride, arsenic, anabolic steroids, and radiation have all been mentioned in etiopathogenesis [2, 22, 23]. It is more common in males and mostly seen in the sixth or seventh decades of life. HAs are biologically very aggressive and often metastatic at the initial diagnosis. Lungs and spleen are the most common sites for metastases [2, 22]. On gross pathological evaluation, the tumor is characterized by remarkable necrosis and intratumoral bleeding [22, 23].

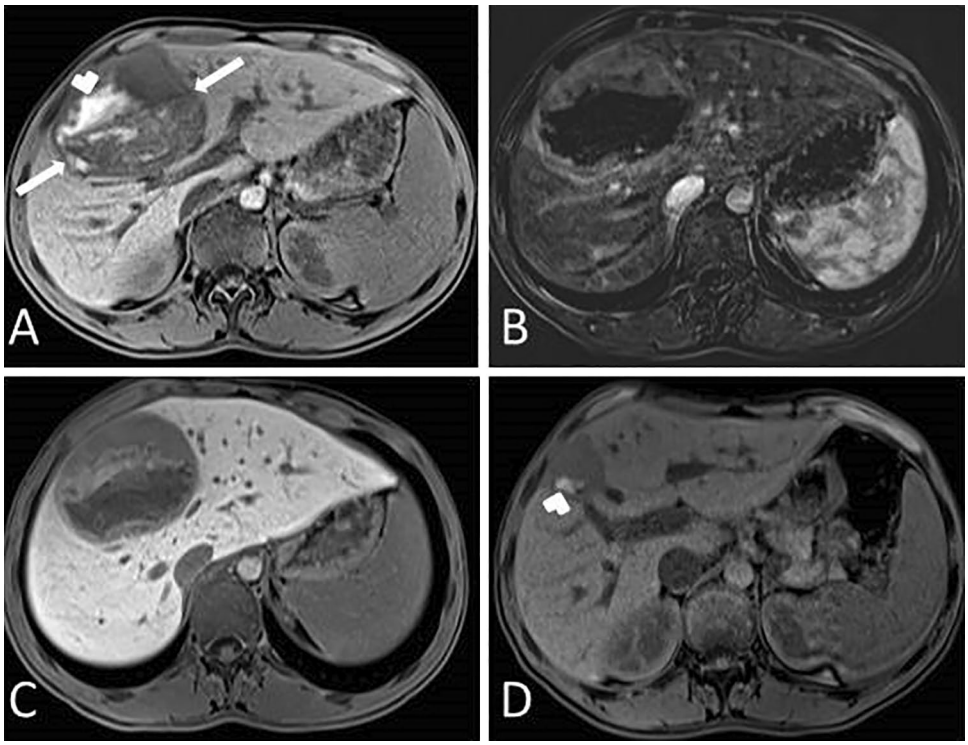

Fig. 5 24-year-old male patient with recently diagnosed Hodgkin lymphoma underwent an abdominal MRI exam. **A** Axial precontrast T1W fat-saturated MR image demonstrates a large mass (arrows) with internal hemorrhage (arrowhead) in the liver. The lesion shows peripheral enhancement on arterial phase (**B**) and is hypointense on HBP (**C**). Histopathological findings revealed hepatic adenoma. **D** Follow-up imaging study demonstrated the decrease in lesion size with a small residual hemorrhagic focus (arrowhead)

On CT studies, the tumor appears mostly hypodense on nonenhanced phase and hypoenhancing on postcontrast images. Unusual angiosarcomas may appear hyperenhancing tumors and mimic cavernous hemangiomas or other hypervascular tumors on single-phase imaging [22]. Multiphasic dynamic studies may be helpful to differentiate these HAs from hemangiomas or HCCs. On MRI, HAs are mostly hemorrhagic with heterogeneous internal enhancement (Fig. 6). Internal hyperintensity on precontrast T1W MR images and fluid–fluid levels on T2W images are highly suggestive for intratumoral bleeding [22]. Spontaneous tumor rupture is a potentially lethal complication of these tumors and may cause a significant amount of hemoperitoneum. Free tumor spillage into the peritoneal cavity after spontaneous hemorrhage may also cause peritoneal angiosarcomatosis [24–26].

Non-neoplastic bleeding

Hepatic cyst

Hepatic cysts (HC) are among the most common benign liver lesions, with an estimated prevalence of 2.5% in the general population [27]. HCs may be solitary or multiple. Patients with multiple HCs should be evaluated for polycystic liver disease, typically associated with polycystic kidney disease. HCs are usually asymptomatic and incidentally diagnosed [27, 28].

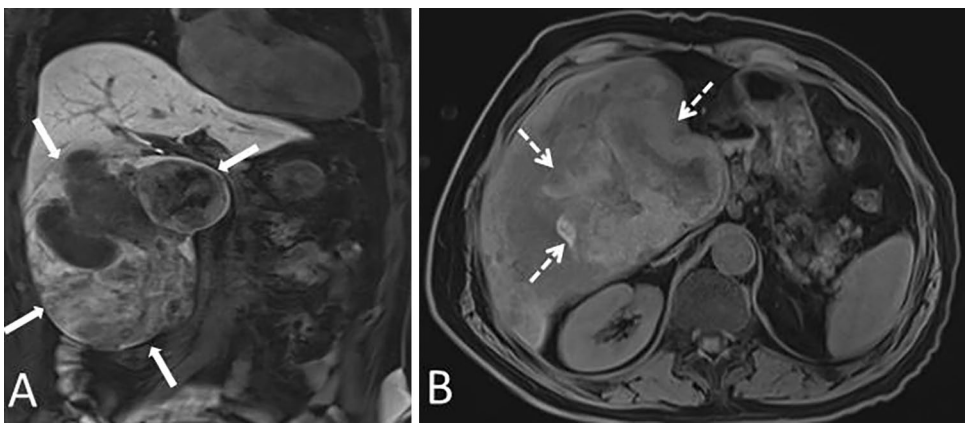

Fig. 6 54-year-old male patient presenting with weight loss. **A** Axial postcontrast T1W MR image shows a heterogeneously enhancing large mass in the liver (arrows). **B** Axial precontrast T1W MR image demonstrates central large hemorrhagic component (dashed arrows). Histopathological confirmation revealed angiosarcoma

On imaging, HCs follow typical imaging characteristics of cysts elsewhere in the body. Intracystic hemorrhage is a rare complication of the HCs and may present with right upper quadrant pain. In this case, HCs may demonstrate heterogeneous hyperattenuation, fluid–fluid level, and internal septations on CT. On MRI, high signal intensity on precontrast T1W images and associating low signal intensity on T2W images are typical [2, 27, 28]. MRI studies with subtraction images may be helpful in these patients to differentiate HCs from cystic tumors, which may contain solid mural parts (Fig. 7).

Miscellaneous conditions

Although the most common cause of spontaneous hepatic hemorrhage in patients with cirrhosis is HCC rupture, spontaneous hepatic hemorrhage without malignant changes may also be rarely seen in cirrhosis. The underlying mechanism is either the rupture of macronodular cirrhosis or rupture of the lymphatic vessels and varicose veins due to portal hypertension [29]. Extreme caution should be exercised in these patients not to overlook an underlying HCC.

Pancreas

Neoplastic bleeding

Pancreatic cystic lesions have been frequently detected due to extensive use of cross-sectional imaging. A microcystic lesion in the pancreatic head may suggest serous cystadenoma (SC), whereas macrocystic lesions are more likely to be intraductal papillary mucinous neoplasms (IPMN) or mucinous cystadenomas. Although hemorrhagic intraparenchymal cysts are frequently observed in patients with acute and chronic pancreatitis, spontaneous bleeding has rarely been reported in SCs or IPMNs [30–33]. MRI is superior to other imaging modalities due to its unique soft-tissue resolution, which allows better evaluating the internal structure of SCs and pancreatic duct connection of IPMNs. Blood products typically give an inherent high T1 signal on MRI (Fig. 8).

Pancreatic NETs (pNETs) arising from islet cells constitute 8–10% of all pancreatic cancers [34]. Although sporadic neoplasms may occur, increased risk for pNET is well known in patients with multiple endocrine neoplasm type 1, von Hippel–Lindau, or neurofibromatosis type 1. On cross-sectional imaging, pNETs are usually hypervascular masses owing to their rich capillary network. Calcification, necrosis, hemorrhage, or cystic changes may be found in larger tumors [35, 36]. Hemorrhagic pNETs can be difficult to diagnose;

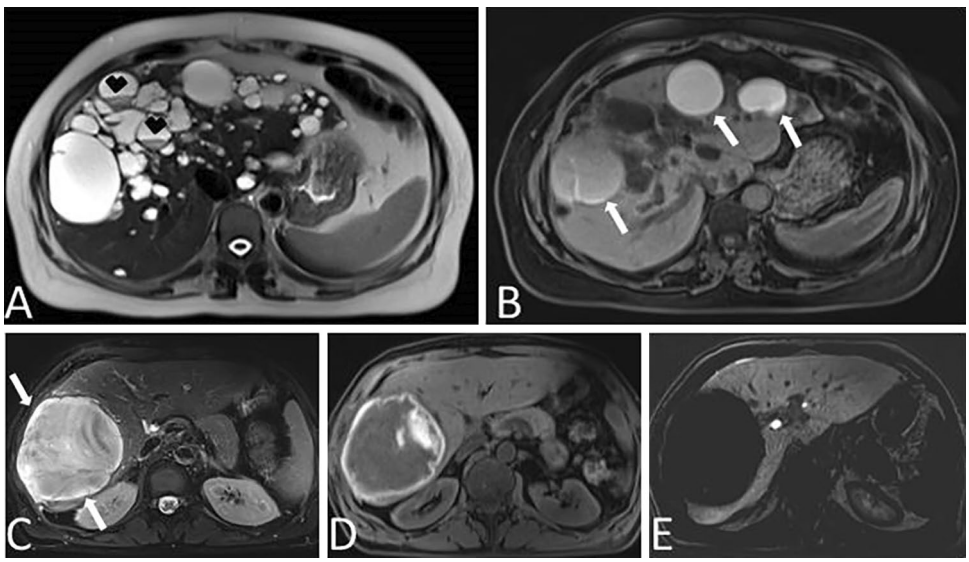

Fig. 7 Hemorrhagic liver cysts in two different patients. **A** 57-year-old female patient with known polycystic liver disease presenting with jaundice and recent-onset right upper quadrant pain. Axial T2W MR image shows multiple liver cysts and two cysts with internal fluid–fluid levels (arrowheads), suggestive of hemorrhage. **B** Axial precontrast T1W MR image demonstrates the hemorrhagic liver cysts (arrows) in the same patient as in **A**. **C**–**E** 50-year-old male patient presenting with abdominal pain. **C** Axial fat-saturated T2W MR image shows a large hyperintense mass in the liver (arrows). **D** Axial precontrast T1W MR image demonstrates internal hyperintense foci suggestive of hemorrhage. **E** There is no enhancement on post-contrast T1W subtraction images. Imaging findings were found to be consistent with a hemorrhagic liver cyst. Follow-up imaging study demonstrated interval decrease in the lesion size (not shown)

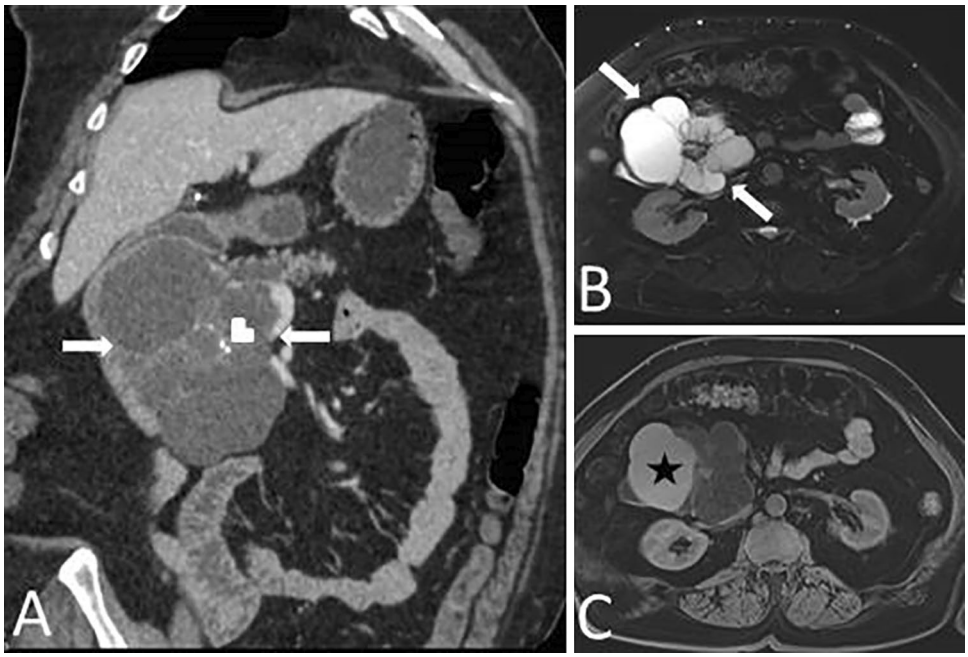

Fig. 8 64-year-old female patient presenting with acute abdominal pain. **A** Coronal postcontrast CT image shows a multiloculated cystic lesion (arrows) in the pancreatic head. Also, note is made of central calcification (arrowhead). **B** Axial T2W MR image better revealed the multiloculated cystic nature of this lesion (arrows). **C** Axial fat-saturated precontrast T1W MR image demonstrates hemorrhagic component (star) of the lesion. Histopathological confirmation after surgical removal revealed hemorrhagic serous cystadenoma

Fig. 9 48-year-old female patient with known MEN-1 syndrome underwent MRI scanning. **A** Axial precontrast T1W MR image shows a hyperintense lesion (arrows) in the pancreatic head. **B** The lesion is hypointense (arrows) on fat-saturated T2W MR image. **C** Axial postcontrast T1W MR image demonstrates peripheral enhancement of the lesion. A nodular enhancement (arrowhead) was also seen within the lesion. Imaging findings were suggestive of a hemorrhagic pNET. Surgical findings confirmed the diagnosis

however, dynamic contrast-enhanced MRI with subtraction images may be helpful by demonstrating the contrast-enhancing solid component or internal septae (Fig. 9).

Non-neoplastic bleeding

Non-neoplastic spontaneous bleeding of the pancreas is mainly related to pseudocysts and peripancreatic pseudoaneurysms, which are well-known complications of acute pancreatitis [36]. According to the revised Atlanta classification, any fluid collection seen 4 weeks after the onset of the disease is considered as a pseudocyst in patients with a history of interstitial edematous pancreatitis [37]. On imaging, a pseudocyst is an irregularly marginated or well-circumscribed cystic lesion depending on its stage. Blood products may be seen within the lesion, which may cause T1 signal hyperintensity on MRI and high-attenuation on unenhanced CT [30].

Spontaneous rupture has also been described in some uncommon pancreatic lesions, such as pancreatic endometrioma [38]. In such lesions, hyperdense fluid or fluid–fluid level on unenhanced CT and high T1 signal intensity on MRI may be found, reflecting the hemorrhagic composition. A pancreatic lesion with peripancreatic or perisplenic hemorrhagic fluid collection may suggest tumor rupture; however, in such circumstances, preoperative diagnosis of the tumor type may be impossible (Fig. 10).

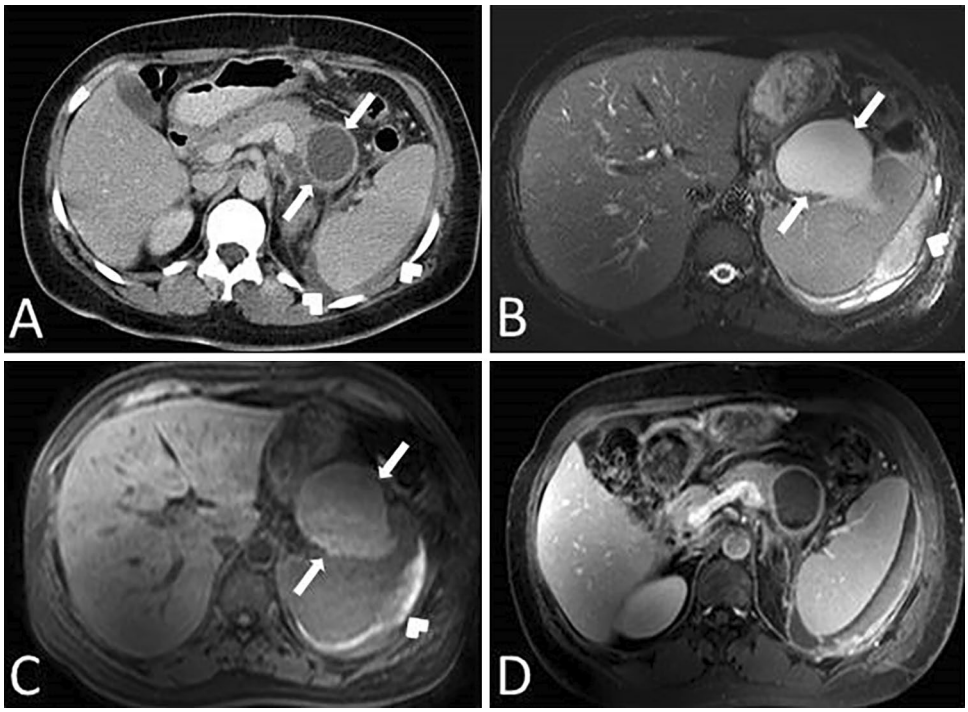

Fig. 10 38-year-old female patient presenting with acute onset epigastric pain. Axial postcontrast CT (**A**) and T2W MR (**B**) images show a cystic mass within the pancreatic tail (arrows) and associated subcapsular splenic fluid collection (arrowheads). **C** Axial precontrast T1W MR image delineates hemorrhagic nature of the lesion (arrows) and subcapsular splenic hematoma (arrowhead). **D** Axial postcontrast T1W MR image shows no apparent mural enhancement within the cyst. Histopathological findings after surgical extirpation revealed pancreatic endometrioma

Spleen

Neoplastic bleeding

The most common malignant tumors of the spleen are metastases, with hematopoietic tumors being the most common. Metastases from solid tumors are relatively uncommon. The most common solid tumors that metastasize to the spleen are melanoma, breast, lung, ovary, pancreas, and colon cancers. Metastases are usually hypodense on contrast-enhanced CT and hypointense on contrast-enhanced T1W MR images. Hemorrhage may be detected in metastases from solid tumors such as RCC [39, 40].

The most common primary tumor of the spleen associated with hemorrhage is, although rare, angiosarcoma. Tumor rupture is not rare in these patients, with a reported prevalence of 25% [40]. Metastatic foci within liver parenchyma are commonly detected at the initial diagnosis. On cross-sectional imaging, these tumors are typically heterogeneously hyperenhancing masses with internal necrosis and hemorrhage. These imaging features characteristically reflect the biologically aggressive nature of these tumors. Perisplenic hematoma, hemoperitoneum, or intraperitoneal tumor spillage may occur as a consequence of tumor rupture

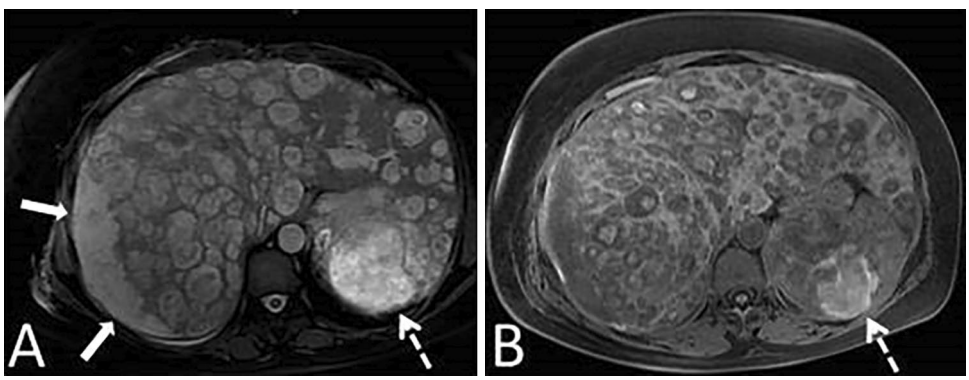

Fig. 11 42-year-old female patient with upper abdominal pain. **A** Axial T2W MR image shows multiple target-like lesions in the liver and spleen. Associating subcapsular fluid collections in the liver (arrows) and spleen (dashed arrow) suggest tumor rupture. **B** Axial T1W MR image depicts hemorrhagic nature of lesions. Note the hyperintensity of the splenic subcapsular fluid collection (dashed arrow). Lesions were found to represent metastatic angiosarcoma of the spleen

(Fig. 11) [39–41]. Despite the fact that solitary or multiple splenic masses with concomitant liver metastases may also be detected in patients with metastases from different primary sources, the clinical history and internal features of the tumor may be helpful for diagnosis.

Non-neoplastic bleeding

Splenic epidermoid cysts (EC) are thought to be congenital lesions. The etiopathogenesis is related to fluid entrapment between the peritoneal mesothelial infoldings. It accounts for approximately 10% of all splenic cystic lesions and is mostly asymptomatic. On US, they are anechoic with low-level internal echoes reflecting cholesterol deposition. On CT or MRI, ECs follow the typical imaging characteristics of cysts detected elsewhere in the body [42]. Despite being rare, rupture of ECs may occur. A hemorrhagic lesion with associating subcapsular hematoma or hemoperitoneum may be detected on CT or MRI when rupture happens (Fig. 12). The absence of detectable enhancement in contrast-enhanced studies is usually sufficient in differentiating ECs from other hemorrhagic splenic lesions [43, 44].

Spontaneous splenic rupture is an infrequent complication in patients with sickle cell anemia and patients on anticoagulation treatment. The potential underlying mechanism in sickle cell anemia is splenic infarct with subcapsular hemorrhage and subsequent rupture. These patients may be hemodynamically unstable, and CT is the preferred imaging modality for diagnosis. On CT, spontaneous splenic rupture is diagnosed with detection of a subcapsular hematoma or hemoperitoneum with accompanying intrasplenic infarcts (Figs. 13, 14) [45].

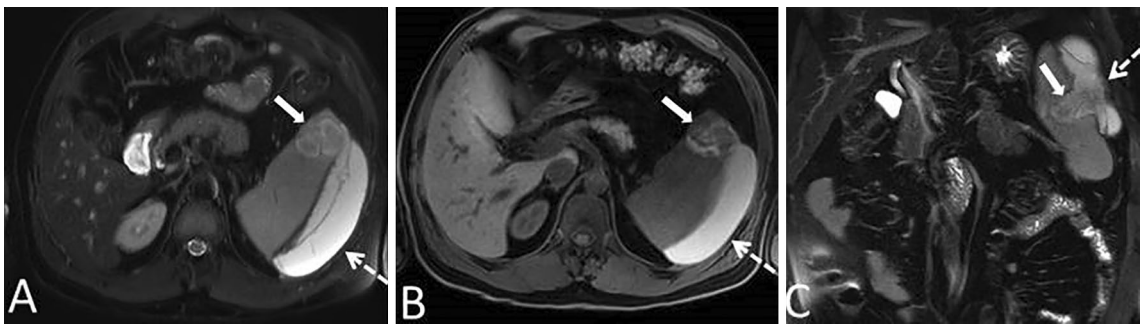

Fig. 12 44-year-old male patient presenting with acute left upper quadrant pain. On US, hypoechoic subcapsular fluid collection encircling the spleen and an intraparenchymal mass of heterogenous echotexture were found (not shown). Axial T2W (**A**) and precontrast fat-saturated T1W (**B**) MR images show subcapsular splenic hematoma (dashed arrows) and a hemorrhagic lesion (arrows) in the spleen. **C** Coronal T2W MR image better demonstrates the continuity between the lesion (arrow) and subcapsular hematoma (dashed arrow). No discernible enhancement was detected on postcontrast-subtracted MR images (not shown). Surgical findings revealed the rupture of a splenic epidermoid cyst

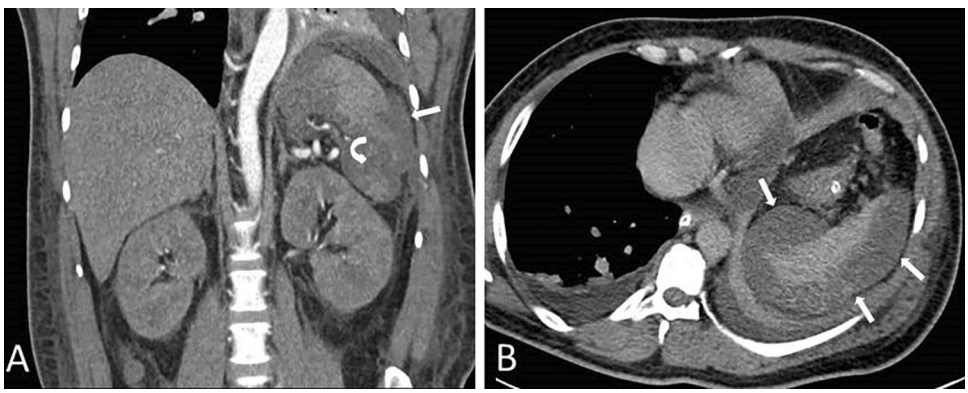

Fig. 13 39-year-old male patient with known sickle cell anemia presenting with acute left upper quadrant pain. **A** Coronal postcontrast CT image shows subcapsular splenic fluid collection (arrow) and splenic infarction (curved arrow). **B** Axial postcontrast CT image better demonstrates subcapsular splenic fluid collection (arrows). Imaging findings were found to be consistent with spontaneous splenic rupture

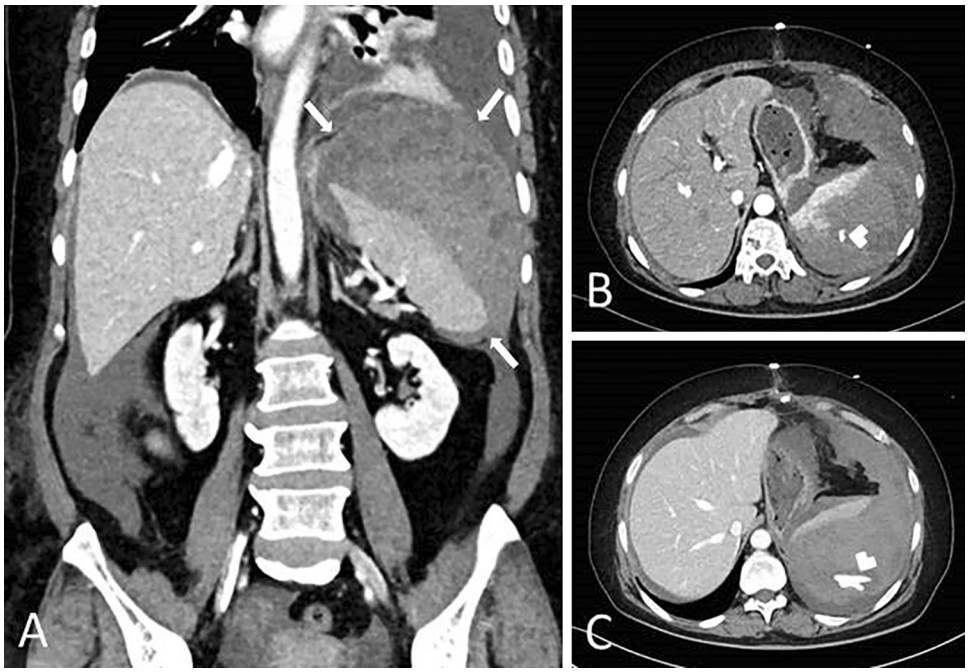

Fig. 14 67-year-old female patient on chronic warfarin treatment presents with acute left upper quadrant pain. Laboratory evaluation revealed a significant increase in INR (higher than 10). **A** Coronal contrast-enhanced CT image shows a large subcapsular splenic hematoma (arrows). **B** Axial contrast-enhanced arterial phase CT image demonstrates the contrast media extravasation (arrowhead) consistent with active bleeding. **C** Extravasated contrast increased on venous phase (arrowhead)

Fig. 15 35-year-old male patient presenting with severe left upper quadrant pain. On US, a large perinephric hematoma was found in the left kidney (not shown). Coronal postcontrast CT image shows the large perinephric hematoma (arrow) and accompanying renal mass (dashed arrow). Also, note is made of multiple parenchymal nodules (arrowheads) in lung bases, suggestive of metastatic disease. Histopathological confirmation of a lung nodule revealed metastatic papillary RCC

Kidney

Neoplastic bleeding

Renal cell carcinoma

RCC is the most common malignant renal tumor, with clear cell carcinoma being the most common subtype. Also, RCC is the most common malignant renal neoplasm associated with intratumoral hemorrhage or perirenal hematoma (Fig. 15). In addition, hematuria may be observed in cases where the tumor extends into the renal pelvis (Fig. 16) [46–48]. The tumor subtype is not a good predictor of hemorrhage, as both clear cell RCC and papillary RCC, the most common subtypes, usually contain hemorrhagic areas. Also, unlike angiomyolipoma (AML), tumor size is not a reliable predictor for bleeding in RCCs. Rarely, an arteriovenous fistula may develop within larger tumors, which may increase the risk of spontaneous bleeding. Tumor thrombus in renal veins may also predispose the tumor to bleed due to increased intratumoral pressure [49].

Angiomyolipoma

AML is the most common solid benign renal tumor. Histopathologically, it consists of variable amounts of disorganized vessels, fat, and smooth muscle. Although the vast majority of AMLs occur sporadically, 20% of cases are associated with tuberous sclerosis. In these patients, AMLs tend to occur multiple and are larger in size. Imaging-based diagnosis is usually straightforward if macroscopic fat is

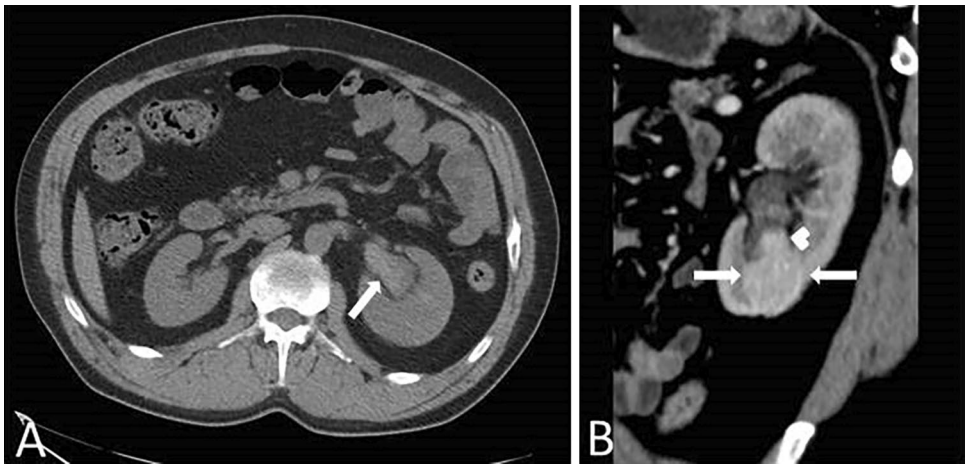

Fig. 16 54-year-old male patient presenting with acute gross hematuria underwent a CT urography examination. **A** Unenhanced CT image shows hyperdense content in the renal pelvis (arrow) reflecting blood products. **B** Coronal postcontrast CT image demonstrates an endophytic hypervascular mass (arrows) in lower pole of the left kidney. Note tumor extension into the collecting system (arrowhead). Histopathological confirmation after partial nephrectomy revealed clear cell RCC

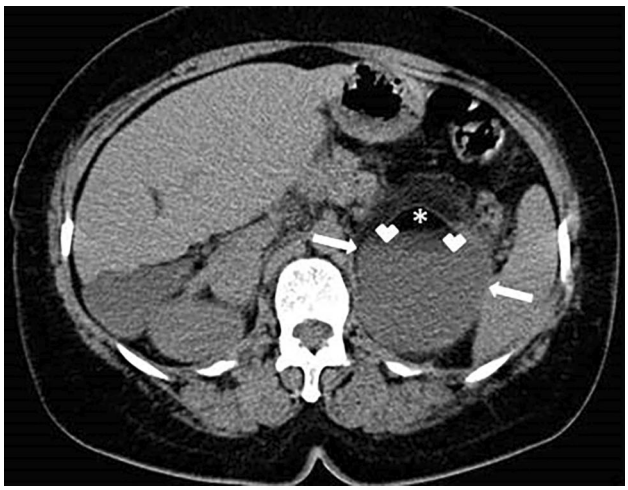

Fig. 17 49-year-old female patient with a known solid mass in the left kidney underwent a CT examination for preoperative planning. Axial precontrast CT image revealed a mass (arrows) containing macroscopic fat (asterisk). An internal fluid–fluid level (arrowheads) was also present, suggestive of intratumoral hemorrhage. The lesion was found to be consistent with angiomyolipoma. Follow-up studies confirmed stability of this lesion

seen; however, lipid-poor AMLs may be difficult to differentiate from RCCs [46]. Spontaneous hemorrhage is a well-known complication of AMLs, commonly occurring in AMLs greater than 4 cm in size (Fig. 17). Pseudoaneurysm may develop within larger lesions due to increased blood flow, and a pseudoaneurysm greater than 5 mm in size tends to bleed spontaneously (Fig. 18) [50]. Hyperdensity and fluid–fluid level on unenhanced CT reflect the intralesional hemorrhage. Perirenal or retroperitoneal hematoma may occur when the lesion ruptures. CT angiography (CTA) is usually the preferred imaging modality in the acute setting. With CTA, both diagnosis and mapping of arterial anatomy are confidently made for planning the endovascular intervention.

Oncocytoma

Oncocytoma is the second most common benign renal neoplasm after AML (3–7% of all renal masses). On imaging, it is usually peripherally located, well-circumscribed, hypervascular solid mass. In approximately half of oncocytomas, a low signal intensity capsule, T2-hyperintense central scar, spoke-wheel enhancement pattern, or segmental enhancement inversion may be identified; however, these findings are not specific and may also be found in RCCs (particularly in the chromophobe subtype) [46, 48]. The imaging-based diagnosis of oncocytoma is usually difficult, and histopathological confirmation is almost always required to differentiate from RCC. The presence of hemorrhage, albeit rare, has been shown in oncocytomas, and this makes differential diagnosis even more challenging [48].

Non-neoplastic bleeding

Renal cyst

Renal cystic lesions are the most commonly encountered renal lesions. Bosniak classification is widely used to separate surgical cystic lesions from non-surgical ones and divides renal cystic lesions into four categories according to their malignancy risk [51]. Patients older than 50 years usually have at least one renal cyst, with Bosniak type 1 or 2 cysts being the most common. Patients are generally asymptomatic, but larger cysts may complicate with infection, hemorrhage, or rupture (Fig. 19). Hemorrhage is a more common complication in patients with polycystic kidney disease. Hemorrhagic cysts are included in Bosniak type 2 or type 2F according to their sizes and locations. A hyperattenuating lesion (> 20 HU) without imperceptible enhancement on CT is considered a hemorrhagic cyst [51, 52]. Fluid–fluid level within a cyst may suggest intracystic hemorrhage, particularly in a patient with acute flank pain.

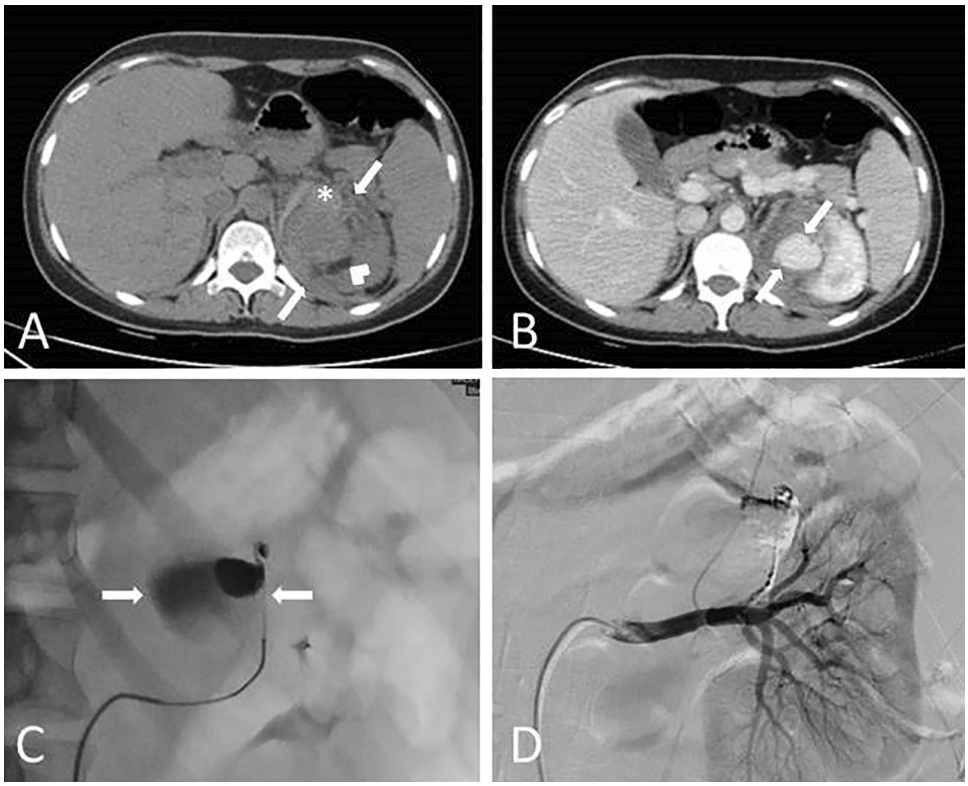

Fig. 18 39-year-old male patient with known tuberous sclerosis and bilateral renal angiomyolipomas presenting with acute left upper quadrant pain. **A** Axial precontrast CT image showed a left kidney angiomyolipoma (arrows) with internal macroscopic fat (arrowhead). Note the hyperdense area within the tumor (asterisk) and perilesional fat stranding suggestive of acute hemorrhage. **B** Axial contrast-enhanced CT image shows a large pseudoaneurysm (arrows) within the lesion. **C** Digital subtraction angiography (DSA) again showed this pseudoaneurysm (arrows). **D** Superselective embolization of this pseudoaneurysm was performed

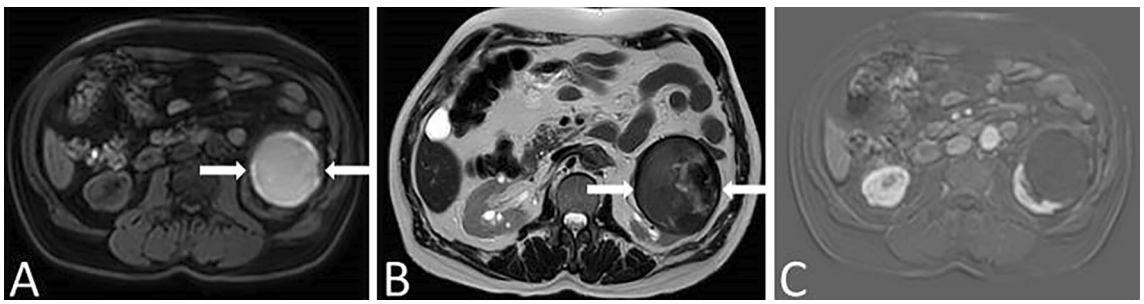

Fig. 19 60-year-old male patient with known colon cancer underwent an MRI examination for recent-onset moderate abdominal pain. **A** Axial precontrast T1W MRI image shows a hyperintense mass (arrows) in the left kidney. **B** The mass is heterogeneously T2-hypointense (arrows). **C** There is no discernible enhancement on postcontrast T1W subtraction images. Imaging findings were found to represent a hemorrhagic renal cyst. Follow-up imaging studies demonstrated interval shrinkage of the lesion

Hematomas in the perirenal and other retroperitoneal planes may also be observed in certain patients with cyst rupture (Fig. 20). In such cases, it may be challenging to identify the kidney cyst as the culprit lesion as hematoma may obscure the underlying abnormality.

Coagulopathies

Spontaneous subepithelial hemorrhage, also known as Antopol–Goldman lesion, is an extremely rare cause of painful hematuria in patients with known hemophilia or on warfarin treatment [53]. Multiphase CT urography (CTU) is the preferred imaging approach in patients with hematuria. In the unenhanced images of CTU, Antopol–Goldman lesions are seen as hyperdense mural thickening of the renal pelvis and the upper ureter. In patients with a large hematoma, centrally located hyperdense mass adjacent to the renal pelvis may be detected (Fig. 21). Contrary to TCC, Antopol–Goldman lesions do not demonstrate enhancement after contrast injection. Follow-up CT scans may be necessary to show complete resolution of the lesion after proper treatment [54].

Miscellaneous conditions

Wunderlich syndrome, first described in 1856, is a rare clinical event characterized by spontaneous renal hemorrhage into

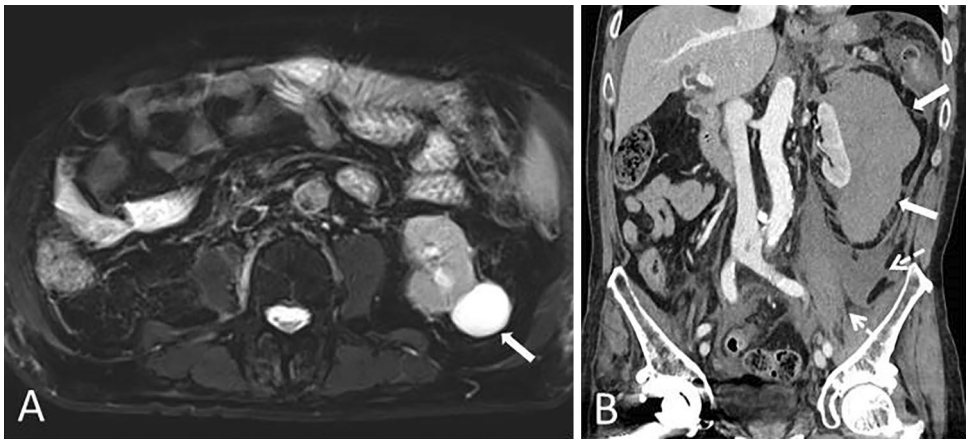

Fig. 20 74-year-old male patient with known left renal cyst presenting with left upper quadrant pain. **A** Axial T2W MR image from a year ago shows the left renal cyst (arrow). **B** Coronal postcontrast image from the current CT study demonstrates a large perinephric hematoma (arrows) and associating retroperitoneal hematoma (dashed arrows). Imaging findings were found to be compatible with acute cyst rupture. Follow-up imaging studies demonstrated complete resolution of the perinephric hematoma without an underlying mass (not shown)

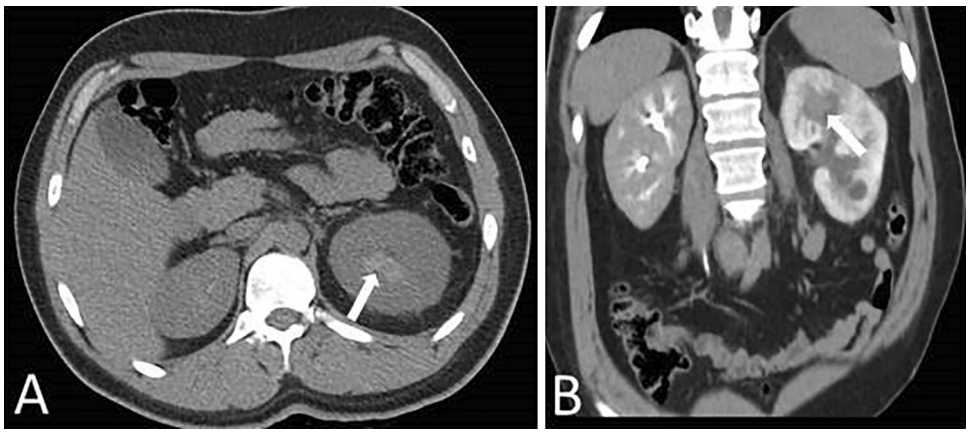

Fig. 21 32-year old male patient with known Hemophilia A presenting with recent-onset painful gross hematuria underwent a CTU examination. **A** Axial precontrast CT image shows a hyperdense mass in the upper pole of the left kidney (arrow). **B** On the postcontrast CT image, the lesion (arrow) did not demonstrate any discernible enhancement. Note the delayed urogram of left kidney. Imaging findings along with the patient's history were considered to represent subepithelial hemorrhage (Antopol–Goldman lesion). Follow-up studies demonstrated complete resolution of the lesion (not shown)

the perinephric or subcapsular space. A variety of underlying causes have been identified, including renal neoplasms, hypertension, diabetes mellitus, chronic kidney disease, infections, vasculopathy, and vasculitis. When renal neoplasms are excluded, other causes are extremely rare (Figs. 22, 23) [55, 56].

Bladder

Neoplastic bleeding

Bladder cancer is the most common primary malignant

Fig. 22 44-year-old male patient with known systemic lupus erythematosus presenting with generalized severe abdominal pain. **A** Coronal precontrast CT image shows a large retroperitoneal hematoma (asterisks). **B** Coronal postcontrast CT image demonstrates the contrast media extravasation within the hematoma (arrows) consistent with active bleeding. **C** Digital subtraction angiography (DSA) depicted active bleeding from a renal artery branch (arrow). **D** Superselective embolization was performed with subsequent control of the bleeding

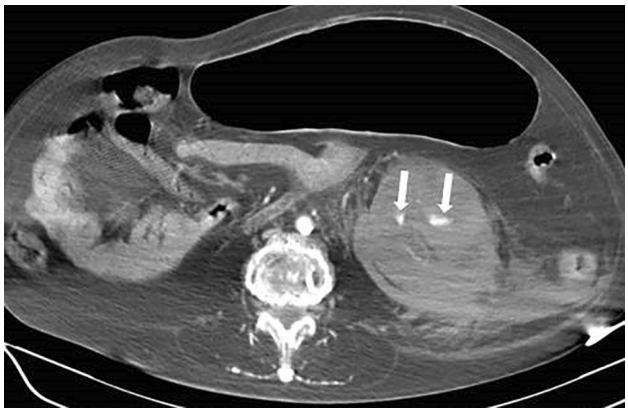

Fig. 23 80-year-old female patient hospitalized for pneumonia and subsequent septic shock underwent CTA for evaluating the cause of acute hemoglobin drop level. Axial arterial phase CT image shows contrast media extravasation into the collecting system of the left kidney (arrows) and perirenal fat stranding. Note the delayed corticomedullary phase of the left kidney

neoplasm of the urinary tract, with TCC being the most common subtype. It is more common in males and mostly seen in the sixth decade of life. Exposure to several chemicals, smoking, bladder stones, chronic infection, and pelvic radiation have all been mentioned in the etiopathogenesis of TCC. Patients usually present with gross painless hematuria [57, 58]. The presence of gross hematuria is a very concerning sign of a urinary neoplasm, and these patients usually undergo both cystoscopy and CTU examination. In addition to confirming bladder cancer, CTU also allows local staging and detection of distant metastases in the abdomen [57]. The presence of endocavitary bladder hematoma associated with the neoplastic lesion is a common finding in these patients (Fig. 24).

Non-neoplastic bleeding

Spontaneous bladder hematoma may be seen in patients with known bleeding diathesis or on anticoagulant therapy. Similar to patients with TCC, those patients also present with gross hematuria and usually undergo a CTU examination. The absence of enhancement and no obvious attachment to the bladder wall may help in differentiating hematomas from TCCs (Fig. 25). Also, mobility of the lesion in US may suggest hematoma [58]. Despite all these mentioned imaging findings, cystoscopic evaluation is almost always needed to rule out a small focus of TCC in these cases.

Adrenal gland

Neoplastic bleeding

Adrenal lesions are usually incidentally detected masses (incidentalomas) during imaging for other purposes. Most of incidentalomas are benign non-functioning adenomas and are easily diagnosed with adrenal CT protocols or chemical shift MRI. Several malignant lesions may also affect the adrenal gland, with metastases being the most common in adults [59]. Despite the fact that several benign and malignant diseases, including adenoma, metastases, neuroblastoma, adrenocortical carcinoma (ACC), pheochromocytoma, and lymphoma, have been reported as a cause for spontaneous hemorrhage, ACC appears to be most common among all these (Figs. 26, 27, 28) [59, 60]. The presence of contrast-enhancing solid portion, calcification, or FDG uptake within hematoma may suggest an underlying adrenal mass, but a definitive diagnosis may be difficult as the lesions may be similar in appearance.

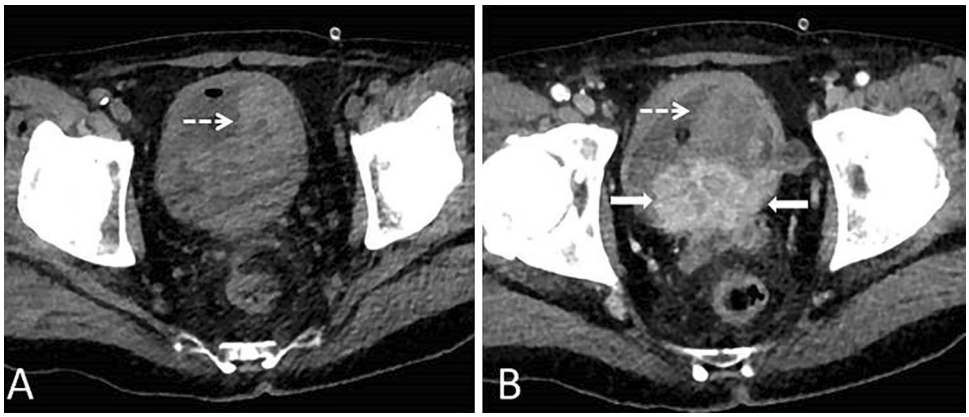

Fig. 24 70-year-old male patient presenting with acute onset gross hematuria underwent a CTU examination. **A** Axial precontrast CT image shows hyperdense structure within the bladder lumen (dashed arrow), suggestive of hematoma. **B** Axial postcontrast CT image demonstrates a contrast-enhancing mass in the posterior wall of the bladder (arrows) and accompanying bladder hematoma (dashed arrow). Histopathological examination after cystoscopy and biopsy revealed TCC

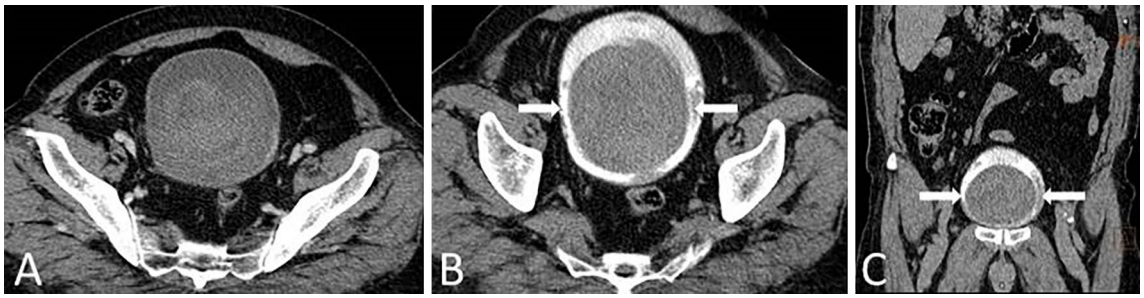

Fig. 25 70-year-old male patient on chronic warfarin treatment presenting with acute gross hematuria. **A** Axial unenhanced CT image shows hyperdense structure within the bladder lumen. Axial (**B**) and coronal (**C**) urographic phase images demonstrate a large mass within the bladder lumen (arrows). There was no discernible enhancement of the bladder mass and no obvious attachment to the bladder wall. Imaging findings were suggestive of a hematoma. No mass was detected in the subsequent cystoscopy

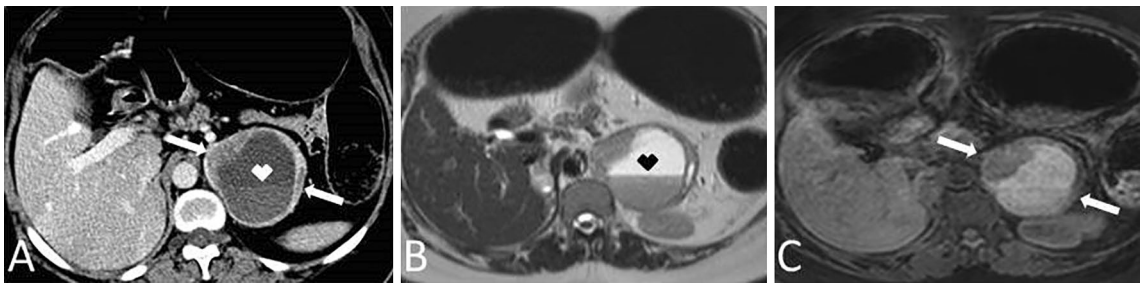

Fig. 26 33-year-old female patient with known multiple endocrine neoplasia syndrome type 2B presenting with severe hypertension. **A** Axial postcontrast CT image shows a thick-walled cystic mass in the left adrenal gland (arrows). A fluid–fluid level (arrowhead) was also present due to intratumoral hemorrhage. **B** The fluid–fluid level (arrowhead) is noted again on T2W MR image. **C** Axial precontrast T1W MR image shows the hemorrhagic mass as mostly hyperintense (arrows). Histopathological confirmation after surgical removal revealed hemorrhagic adrenal pheochromocytoma

Non-neoplastic bleeding

Adrenal gland is supplied by around 50–60 small arteries and drained by a few veins. This unique anatomy is thought to make it prone to spontaneous bleeding [61]. Anticoagulant therapy, antiphospholipid antibody syndrome, and metabolic stress (such as neonatal stress, sepsis, hypotension) have all

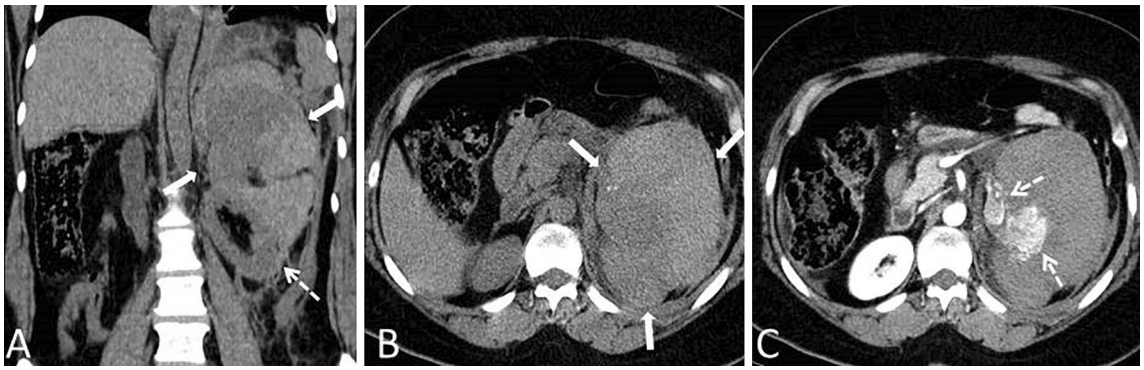

Fig. 27 42-year-old female patient presenting with left upper quadrant pain. Coronal (**A**) and axial (**B**) unenhanced CT images show a large hematoma in the left adrenal region (arrows) and associated retroperitoneal hematoma (dashed arrow in **A**). The adrenal gland could not be visualized separately from this large hematoma. **C** Axial arterial phase postcontrast CT image demonstrates contrast media extravasation consistent with active bleeding. Histopathological examination after emergency surgery confirmed adrenocortical carcinoma

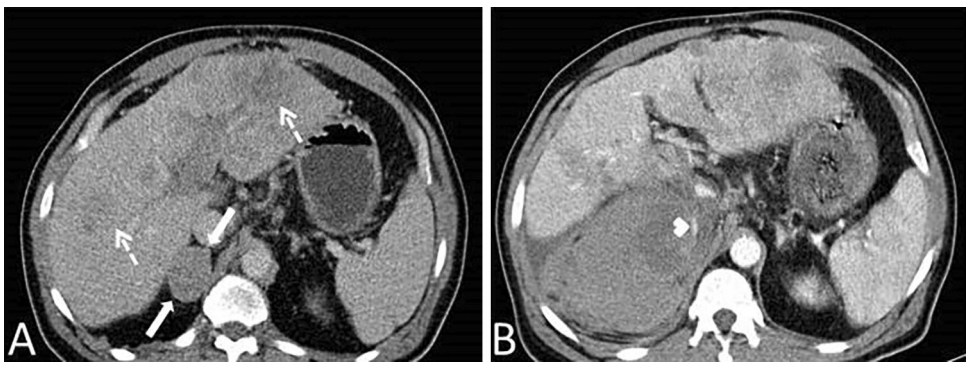

Fig. 28 58-year-old male patient with known HCC. **A** Axial postcontrast CT image shows liver masses (dashed arrows) and right adrenal mass (arrows). The patient presented with severe, acute right upper quadrant pain 15 days after this CT scan. **B** Axial postcontrast CT image showed interval enlargement of the adrenal lesion with a small focus of contrast media extravasation (arrowhead). Imaging findings were found to represent tumoral hemorrhage. Emergency surgery confirmed hemorrhagic metastatic HCC

been mentioned in the etiology of spontaneous adrenal bleeding. Idiopathic bleeding has also been reported [60].

On imaging, an adrenal hematoma is similar to hematomas elsewhere in the body (Fig. 29). In patients with spontaneous adrenal bleeding, great caution should be exercised to rule out an underlying mass. The absence of the contrast-enhancing component on dynamic contrast-enhanced MRI with subtraction images and no FDG-uptake within the hematoma may be helpful in the differential diagnosis. However, even in these cases, an underlying neoplastic process may not be definitely excluded, and follow-up imaging should be planned to confirm interval resolution.

Gastrointestinal tract

Neoplastic bleeding

Acute gastrointestinal (GI) bleeding is a common urgent condition that may be life-threatening. While the most common cause of acute upper GI bleeding (above the ligament of Treitz) is peptic ulcer, diverticulosis is the most common underlying reason for the lower GI system. GI system tumors usually present with anemia due to occult bleeding and are relatively less common causes of acute

Fig. 29 44-year-old male patient with no known past medical history presents with acute onset left upper quadrant pain. **A** Axial unenhanced CT image shows a hyperdense mass in the left adrenal gland (arrows) with associating periadrenal fat stranding. No discernible enhancement was seen on postcontrast images (not shown). The lesion represented either a ruptured mass or an idiopathic adrenal hematoma. The patient was hemodynamically stable, and close imaging and clinical follow-up were concluded. **B** Axial T2W MR image four months after the initial presentation demonstrates almost complete regression of the hematoma (arrows) with no associated underlying mass

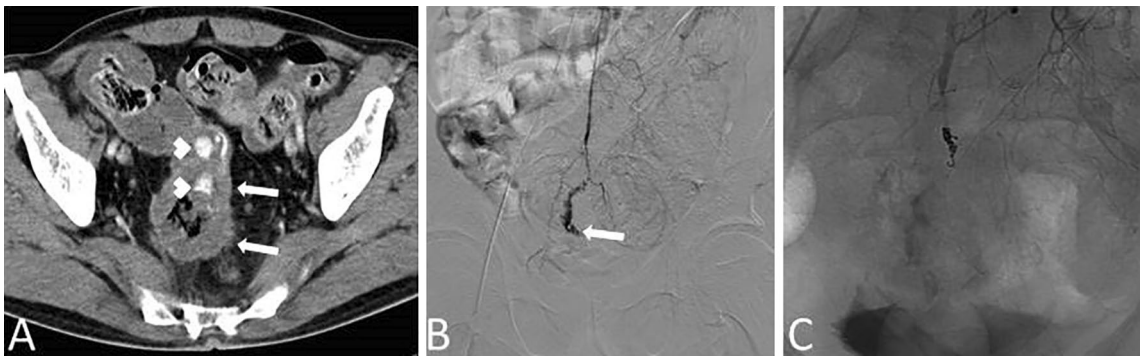

Fig. 30 48-year-old male patient presenting with hematochezia. **A** Axial postcontrast CT image shows diffuse wall thickening of the rectum (arrows) and contrast media extravasation into the lumen consistent with active bleeding (arrowheads). **B** DSA image shows active bleeding from a branch of the inferior mesenteric artery (arrow). **C** Bleeding control was achieved by superselective embolization of the artery with detachable coils. Subsequent colonoscopic biopsy was confirmed rectal adenocarcinoma

GI bleeding. Patients with overt GI bleeding may present with hematemesis, melena, or hematochezia, depending on the bleeding site and severity [62]. CTA with unenhanced, arterial, and venous phases has been widely used in the clinical setting of acute GI bleeding to evaluate the underlying cause and location of the source. Active contrast extravasation from the site of bleeding is a very important and valuable finding as it is helpful to guide endovascular treatment planning. On precontrast images, intraluminal hematomas tend to appear hyperdense. In the arterial and venous phases, endoluminal contrast extravasation may be detected in patients with active bleeding (Fig. 30). Oral contrast use is mostly not preferred in these examinations, as oral contrast may hinder the observation of active contrast extravasation.

Non-neoplastic bleeding

A variety of common and uncommon non-neoplastic causes of GI bleeding have been identified on CTA. GI angiodysplasias that consist of thin-walled blood vessels is an unusual cause for overt GI bleeding. GI angiodysplasias may be seen throughout the GI tract and tend to be multifocal; however, antimesenteric borders of the caecum and right-sided colon are the most common harboring sites. Imaging findings of active bleeding from angiodysplasias are similar to those

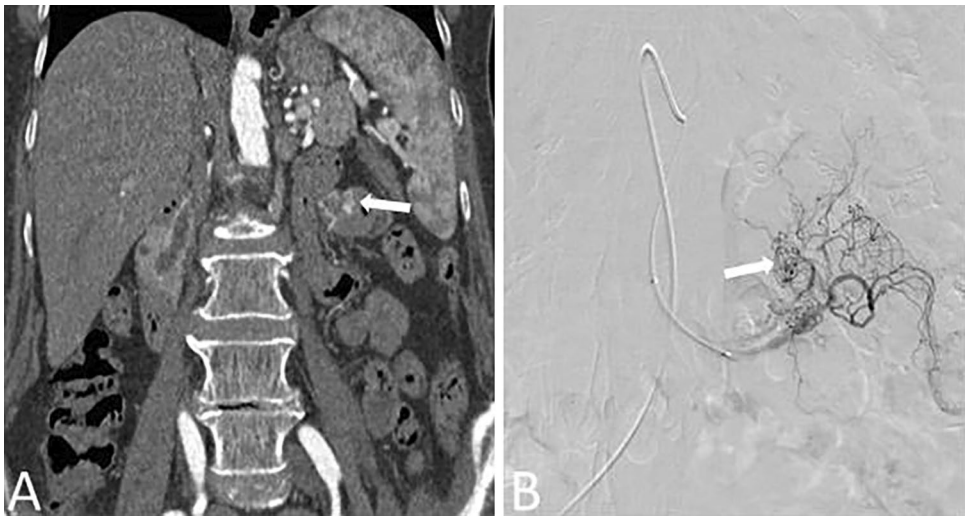

Fig. 31 75-year-old female patient presented with melena. She was hemodynamically stable. Upper and lower GI endoscopic studies were found to be unremarkable. An abdominal CTA was planned for assessment of the underlying cause. **A** Coronal arterial phase postcontrast CT image shows accumulation of vessels in the jejunum wall (arrow) suggestive of angiodysplasia. **B** DSA image demonstrates the angiodysplasia as disorganized ectatic vessels (arrow)

Fig. 32 73-year-old female patient on chronic warfarin treatment presents with abdominal pain. Laboratory evaluation revealed high levels of INR (higher than 10). Axial unenhanced CT image shows hyperdense mural thickening of the ileum (arrows) considered an intramural hematoma

of other causes, but the diagnosis is usually straightforward as they have distinct imaging features. The typical suggestive imaging findings on CTA are focal punctate areas of enhancement in the bowel wall with the early filling of an antimesenteric vein (Fig. 31) [63].

Patients on anticoagulant therapy may present with acute GI bleeding. Spontaneous intramural small-bowel hematomas may also be seen in overcoagulated patients with warfarin. These patients may present with abdominal pain or intestinal obstruction. Intraluminal or intramesenteric hemorrhage or hemorrhagic ascites may be other associating findings. In precontrast images of the CTA, detection of hyperdense mural thickening is a highly suggestive finding for intramural hematoma (Fig. 32) [64]. Despite being rare, spontaneous intramural duodenal hematoma may associate with acute or chronic pancreatitis (Fig. 33) [65].

Gynecological causes

Neoplastic bleeding

Gynecologic malignancies are frequently encountered neoplasms in women, with endometrial carcinoma being the most common, followed by ovarian and cervical cancers. Hormonal, viral, or genetic factors are often associated with gynecological malignancies [66]. Endometrium and cervical cancers mostly present with abnormal vaginal bleeding, whereas ovarian cancer typically causes bloating, constipation, or pelvic pain. Although spontaneous intraabdominal bleeding appears to be rare in patients with gynecological malignancies, invasion of surrounding organs and erosion of vessels may cause intraperitoneal hemorrhage, hematuria, or GI bleeding (Fig. 34).

Non-neoplastic bleeding

Rupture of an ovarian cyst is the most common cause of spontaneous hemoperitoneum in women of reproductive age [1]. Rupture of an ovarian cyst usually presents with acute pelvic pain. On US, a hemorrhagic ovarian cyst is a thin-walled cyst with fluid–fluid level, low-level echoes, and internal septations. Retracting clot adhering to the cyst wall may mimic a nodule but has no blood flow on color Doppler imaging (Fig. 35). In women of childbearing age, ectopic pregnancy rupture should be considered in patients presenting with acute abdomen and hemoperitoneum. A serum beta-human chorionic gonadotropin level greater than 2000 IU, without any imaging evidence of intrauterine pregnancy, should be considered highly suspicious for ectopic

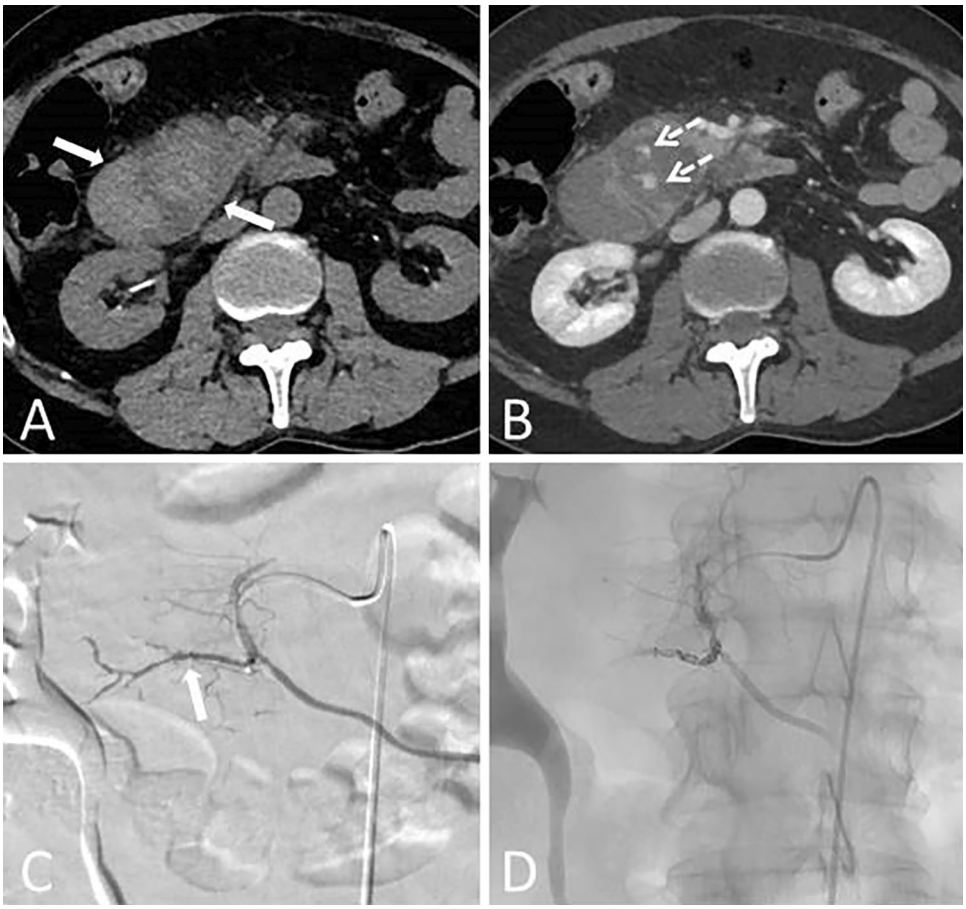

Fig. 33 53-year-old male patient with known chronic pancreatitis presented with recent-onset epigastric pain. **A** Axial unenhanced CT image shows a hyperdense duodenal mass (arrows) suspicious for a mass or hematoma. **B** Axial postcontrast CT image demonstrates contrast media extravasation within this structure consistent with active bleeding (dashed arrows). **C** DSA image shows contour irregularity of a branch of the gastroduodenal artery (arrow) considered the source of active bleeding. **D** Superselective coil embolization was performed to control bleeding. Follow-up imaging studies demonstrated complete regression of the hematoma with no underlying mass (not shown)

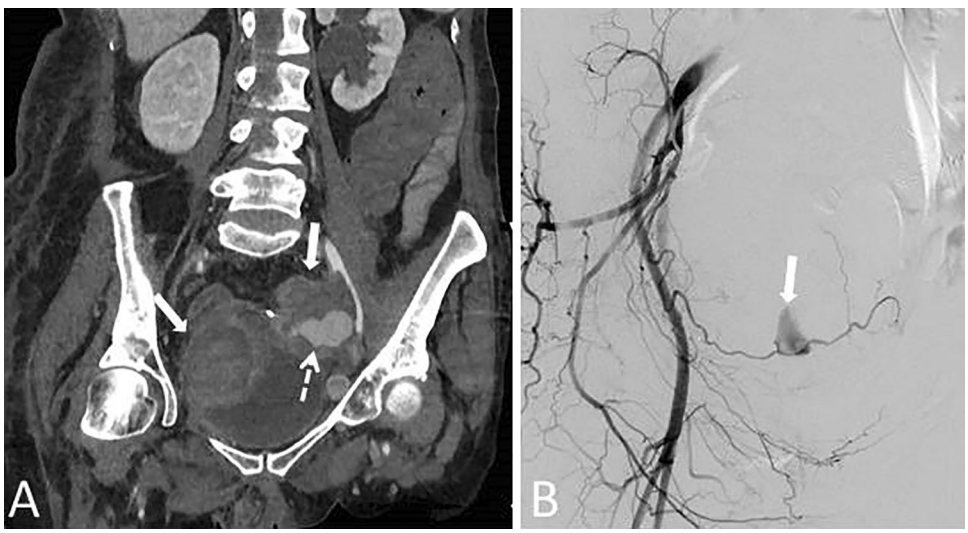

Fig. 34 59-year-old female patient with recurrent endometrial cancer invading bladder wall and sigmoid colon. She now presents with abundant hematuria. **A** Coronal postcontrast CT image shows the pelvic mass (arrows) and active bleeding within it (dashed arrow). **B** DSA image delineates the superior vesical artery as the source of bleeding (arrow). Superselective coil embolization was performed to control active bleeding (not shown)

pregnancy. Tubal ring sign, obvious live extrauterine pregnancy, or a complex extra-adrenal mass with the "ring of fire sign" on color Doppler may be helpful for diagnosis [67].

Despite its rarity, ovarian endometrioma rupture may clinically mimic functional ovarian cyst rupture (Fig. 36) [68]. The presence of a multilocular ovarian cyst with low-level echoes on US may suggest endometrioma; however, dynamic contrast-enhanced MRI with subtraction images may be necessary to exclude underlying malignancy.

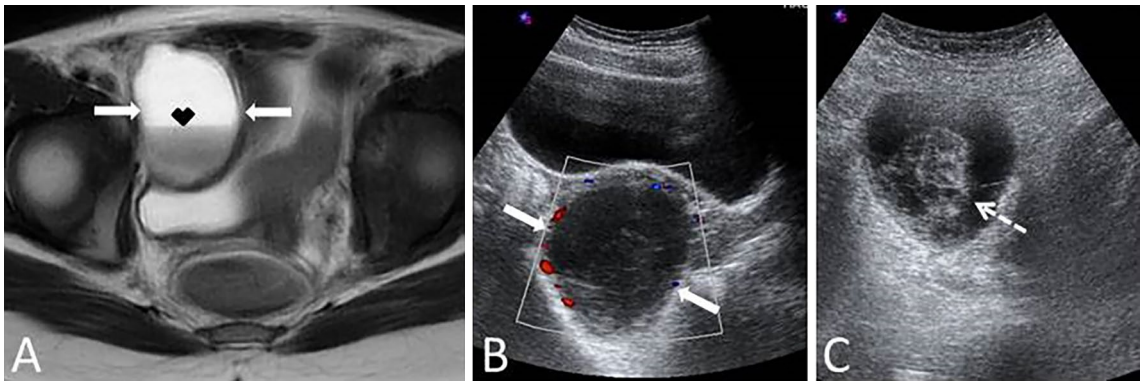

Fig. 35 Hemorrhagic ovarian cysts in two different patients. **A** 20-year-old female patient presenting with pelvic pain. Axial T2W MR image shows a cystic lesion (arrows) with fluid–fluid level (arrowhead) in the right ovary. **B** and **C** 32-year-old female patient presenting with acute onset pelvic pain. On US, a cystic lesion (arrows) with a mural nodule (dashed arrow) was found in the right ovary. No flow signal could be detected within this nodule on color Doppler imaging. Imaging findings were found to be compatible with hemorrhagic ovarian cysts. Follow-up studies showed complete regression of the lesions (not shown)

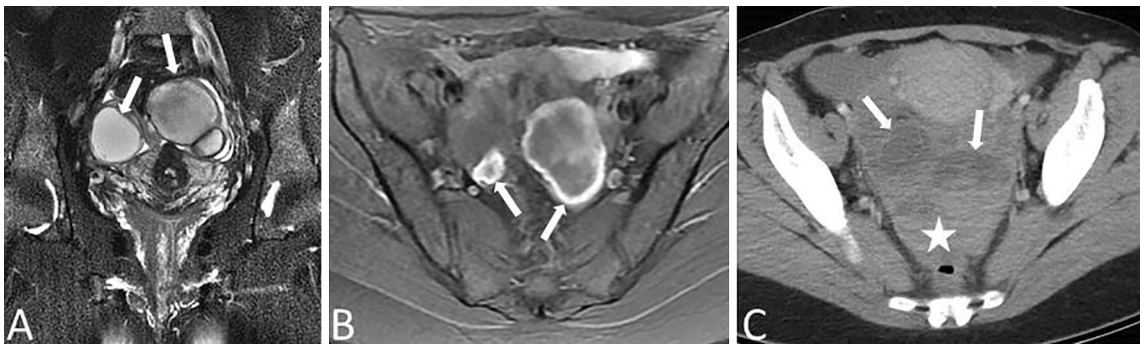

Fig. 36 34-year-old female patient with previously known endometriomas. **A** and **B** Coronal fat-saturated T2W and axial fat-saturated T1W MR images show bilateral ovarian lesions (arrows) consistent with endometriomas. **C** The patient presented with acute onset pelvic pain three months after the first MRI examination. Axial postcontrast CT image shows bilateral ovarian cystic lesions (arrows) and hemoperitoneum (star). Imaging findings along with the patient's medical history were found to be representing endometrioma rupture. Surgical findings confirmed the imaging diagnosis

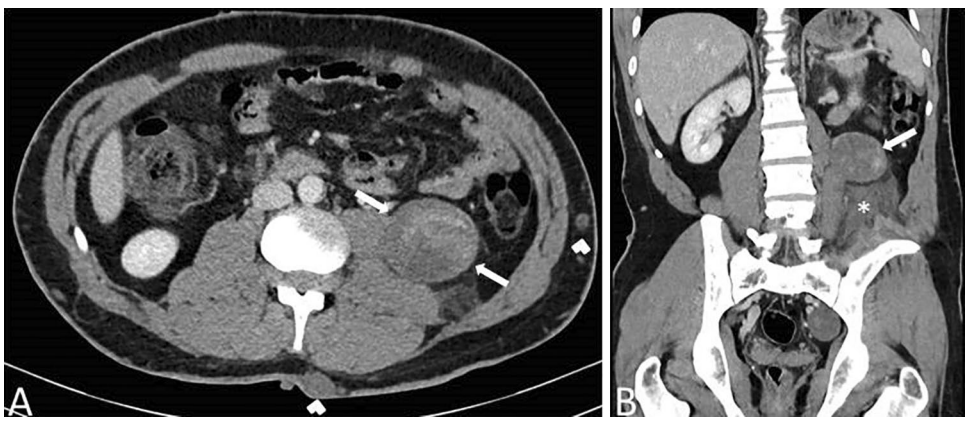

Fig. 37 42-year-old male patient with known neurofibromatosis type 1 presenting with acute, severe left flank pain. Axial (**A**) and coronal (**B**) postcontrast CT images demonstrate a round-shaped mass (arrows) in left retroperitoneum and associated retroperitoneal hematoma (asterisk in **B**). Also, note is made of cutaneous neurofibromas (arrowheads in **A**). Histopathological examination after surgical removal of the lesion revealed neurofibroma

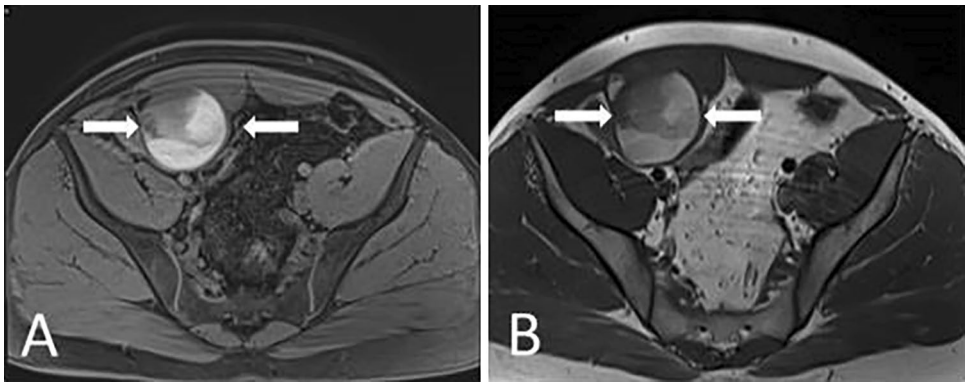

Fig. 38 28-year-old male patient presenting with acute right lower quadrant pain. On US, a heterogeneous mass was found in right lower quadrant (not shown). Axial precontrast T1W (**A**) and T2W (**B**) MR images show a heterogeneous hemorrhagic lesion (arrows) in ileocaecal mesentery. Histopathological examination after surgical removal revealed desmoplastic small round cell tumor

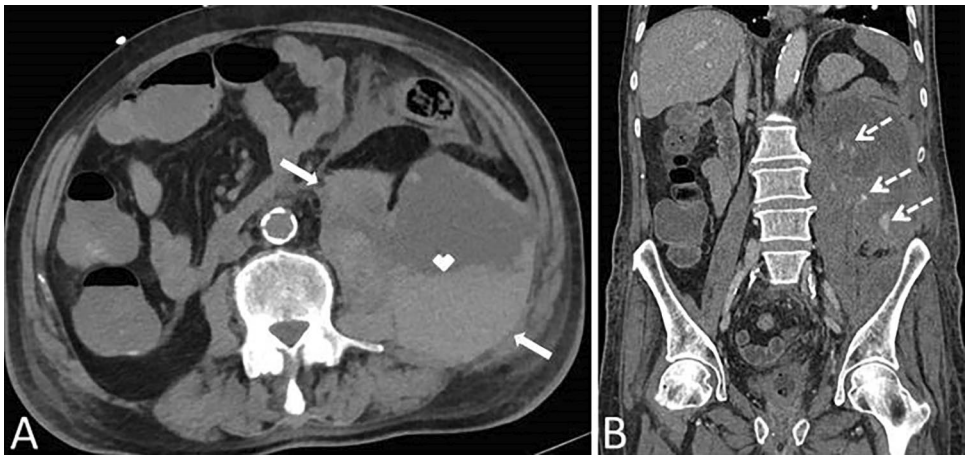

Fig. 39 78-year-old male patient on chronic warfarin treatment presents with acute left flank pain. **A** Axial unenhanced CT image shows a large retroperitoneal hematoma (arrows) with an internal hematocrit level (arrowhead). **B** Coronal postcontrast CT image clearly demonstrates active bleeding (dashed arrows) within this hematoma. The patient was treated with transarterial embolization (not shown)

Mesenteric and retroperitoneal non-parenchymal hemorrhage

Neoplastic bleeding

Mesenteric and retroperitoneal lymph nodes are commonly affected by metastases and lymphoma. Primary mesenteric and non-parenchymal retroperitoneal neoplasms are rare entities, and most of the cases are malignant and mesenchymal in origin. Although some imaging findings, including fat, calcification, necrosis, or myxoid stroma, may provide clues for differential diagnosis, definitive diagnosis of these masses may be extremely challenging and mostly necessitate histopathological evaluation [69]. Spontaneous hemorrhage may be seen in sarcomas, neurogenic tumors, germ cell tumors, metastases, lymphoma, and desmoplastic small round cell tumors (Figs. 37, 38) [70, 71].

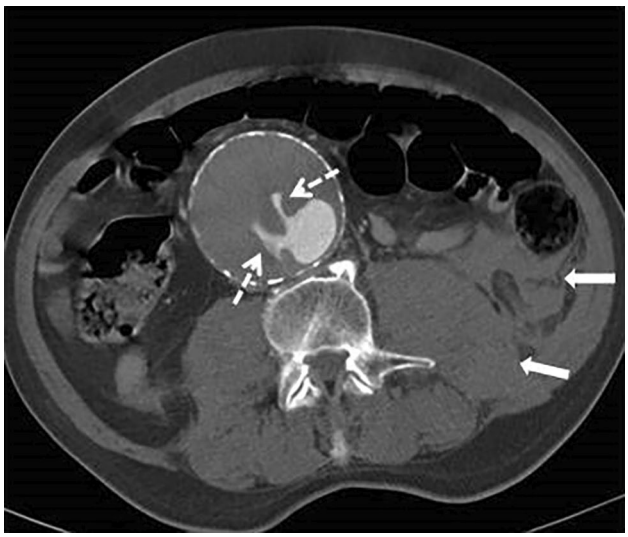

Fig. 40 69-year-old male patient with known abdominal aortic aneurysm presents to the emergency department with acute onset abdominal pain. Axial postcontrast CT image shows the partially thrombosed aneurysm measuring 7.5 cm in diameter. Thrombus fissuration sign (dashed arrows) and associated left retroperitoneal hematoma (arrows) are consistent with aneurysmal rupture. The patient died immediately after this scan

Non-neoplastic bleeding

Coagulopathy-related hemorrhage

Coagulopathy-related spontaneous retroperitoneal bleeding may be seen in patients on anticoagulant or antiplatelet therapy. Symptoms are mostly nonspecific, particularly in elderly patients; however, severe bleeding may manifest with hypovolemic shock [1]. On CT, a large hematoma with an internal hematocrit level is reported to be a sensitive and specific sign for coagulopathic bleeding (Fig. 39) [1]. Clinical history is usually suggestive of the diagnosis; however, an underlying mass should be sought in patients with known malignancy. Follow-up imaging is mandatory for demonstrating the interval resolution of the hematoma, as hematomas may mask the underlying mass on the initial imaging study.

Vascular causes

An abdominal aortic aneurysm may present with abdominal pain and hypovolemic shock in patients with rupture. CTA is the imaging modality of choice to detect aneurysm rupture or other alternative causes of clinical symptomatology. A crescent-shaped hyperdense area in the aneurysm wall reflecting intramural hematoma on unenhanced CT image, increasing aneurysm size, "draped aorta" sign (referring to draping of posterior wall of the aortic aneurysm to anterior surface of the adjacent vertebral body), and "thrombus fissuration sign" (referring to blood dissecting into the mural thrombus) may be indicative for an imminent aneurysm rupture. A large retroperitoneal hematoma adjacent to the aneurysm sac is almost always diagnostic for the rupture (Fig. 40) [1].

Splanchnic artery aneurysms may also be associated with rupture, with hepatic and splenic artery aneurysms being the most common. Despite being rare, spontaneous rupture of celiac and gastroduodenal artery aneurysms have also been reported in the literature [72, 73].

Conclusion

A variety of neoplastic and non-neoplastic conditions may cause spontaneously intraabdominal bleeding. Imaging findings vary depending on the source of bleeding and the underlying cause. Although imaging findings along with the patients' history usually give a clue for diagnosis, imaging-based diagnosis may be challenging, and follow-up studies or histopathological confirmation may be needed.

Author contributions SA and YS: Data collection, manuscript writing, and literature research, ADK: Manuscript editing, project development, supervision, DS, MK, MNÖ: Manuscript editing.

Funding None.

Data availability Not applicable.

Code availability Not applicable.

Declarations

Conflict of interest The authors declare that they have no conflict of interest.

Ethical approval Not applicable.

Consent for publication Not applicable.

Informed consent Not applicable.

References

1. Furlan A, Fakhran S, Federle MP (2009) Spontaneous abdominal hemorrhage: causes, CT findings, and clinical implications. AJR Am J Roentgenol 193:1077–87. https://doi.org/https://doi.org/10.2214/AJR.08.2231
2. Thomas AJ, Menias CO, Pickhardt PJ, Shaaban AM, Gaballah AH, et al (2019) Bleeding Liver Masses: Imaging Features With Pathologic Correlation and Impact on Management. AJR Am J Roentgenol 213:8–16. https://doi.org/https://doi.org/10.2214/AJR.19.21240
3. McEvoy SH, McCarthy CJ, Lavelle LP, Moran DE, Cantwell CP, et al (2013) Hepatocellular carcinoma: illustrated guide to systematic radiologic diagnosis and staging according to guidelines of the American Association for the Study of Liver Diseases. Radiographics 33:1653–68. https://doi.org/https://doi.org/10.1148/rg.336125104
4. Ayuso C, Rimola J, Vilana R, Burrel M, Darnell A, et al (2018) Diagnosis and staging of hepatocellular carcinoma (HCC): current guidelines. Eur J Radiol 101:72–81. https://doi.org/https://doi.org/10.1016/j.ejrad.2018.01.025
5. Bassi N, Caratozzolo E, Bonariol L, Ruffolo C, Bridda A, et al (2010) Management of ruptured hepatocellular carcinoma: implications for therapy. World J Gastroenterol 16:1221–25 https://doi.org/https://doi.org/10.3748/wjg.v16.i10.1221
6. Pinal-García DF, Nuño-Guzmán CM, Gómez-Abarca A, Corona JL, Espejo I (2018) Spontaneous rupture of hepatocellular carcinoma in a young patient with fatal outcome. Case Rep Gastroenterol 12:19–26. https://doi.org/https://doi.org/10.1159/000486193
7. Sahu SK, Chawla YK, Dhiman RK, Singh V, Duseja A, et al (2019) Rupture of hepatocellular carcinoma: a review of literature. J Clin Exp Hepatol 9:245–56. https://doi.org/https://doi.org/10.1016/j.jceh.2018.04.002
8. Shriki JE, Seyal AR, Dighe MK, Yeh MM, Jalikis FG, et al (2015) CT of atypical and uncommon presentations of hepatocellular carcinoma. AJR Am J Roentgenol 205:W411–W23. https://doi.org/https://doi.org/10.2214/AJR.14.14000
9. Jia Z, Tian F, Jiang G (2013) Ruptured hepatic carcinoma after transcatheter arterial chemoembolization. Curr Ther Res Clin Exp 74:41–3. https://doi.org/https://doi.org/10.1016/j.curtheres.2012.12.006

10. Vilgrain V, Boulos L, Vullierme M-P, Denys A, Terris B, Menu Y (2000) Imaging of atypical hemangiomas of the liver with pathologic correlation. Radiographics 20:379–97. https://doi.org/https://doi.org/10.1148/radiographics.20.2.g00mc01379
11. Ribeiro Jr MA, Papaiordanou F, Gonçalves JM, Chaib E (2010) Spontaneous rupture of hepatic hemangiomas: a review of the literature. World J Hepatol 2:428. https://doi.org/https://doi.org/10.4254/wjh.v2.i12.428
12. Casillas VJ, Amendola MA, Gascue A, Pinnar N, Levi JU, Perez JM (2000) Imaging of nontraumatic hemorrhagic hepatic lesions. Radiographics 20:367–78. https://doi.org/https://doi.org/10.1148/radiographics.20.2.g00mc10367
13. Srinivasa S, Lee WG, Aldameh A, Koea JB (2015) Spontaneous hepatic haemorrhage: a review of pathogenesis, aetiology and treatment. HBP (Oxford) 17:872–80. https://doi.org/https://doi.org/10.1111/hpb.12474
14. Silva AC, Evans JM, McCullough AE, Jatoi MA, Vargas HE, Hara AK (2009) MR imaging of hypervascular liver masses: a review of current techniques. Radiographics 29:385–402. https://doi.org/https://doi.org/10.1148/rg.292085123
15. Namasivayam S, Martin DR, Saini S (2007) Imaging of liver metastases: MRI. Cancer Imaging 7:2–9. https://doi.org/https://doi.org/10.1102/1470-7330.2007.0002
16. Sica GT, Ji H, Ros PR (2000) CT and MR imaging of hepatic metastases. AJR Am J Roentgenol 174:691–8. https://doi.org/https://doi.org/10.2214/ajr.174.3.1740691
17. Grazioli L, Federle MP, Brancatelli G, Ichikawa T, Olivetti L, Blachar A (2001) Hepatic adenomas: imaging and pathologic findings. Radiographics 21:877–92. https://doi.org/https://doi.org/10.1148/radiographics.21.4.g01jl04877
18. Klompenhouwer AJ, de Man RA, Thomeer MG, Ijzermans JN (2017) Management and outcome of hepatocellular adenoma with massive bleeding at presentation. World J Gastroenterol 23:4579–86. https://doi.org/https://doi.org/10.3748/wjg.v23.i25.4579
19. Sharma D, Subbarao G, Saxena R (2017) Hepatoblastoma. Proc. Semin Diagn Pathol 34:192–200. https://doi.org/https://doi.org/10.1053/j.semdp.2016.12.015
20. Shelmerdine SC, Roebuck DJ, Towbin AJ, McHugh K (2016) MRI of paediatric liver tumours: How we review and report. Cancer Imaging 16:1–10. https://doi.org/https://doi.org/10.1186/s40644-016-0083-3
21. Pondrom M, Pariente D, Mallon B, Taque S, Branchereau S, et al (2020) Tumor rupture in hepatoblastoma: A high risk factor? Pediatr Blood Cancer 67:e28549. https://doi.org/https://doi.org/10.1002/pbc.28549
22. Koyama T, Fletcher JG, Johnson CD, Kuo MS, Notohara K, Burgart LJ (2002) Primary hepatic angiosarcoma: findings at CT and MR imaging. Radiology 222:667–73. https://doi.org/https://doi.org/10.1148/radiol.2223010877
23. Peterson MS, Baron RL, Rankin SC (2000) Hepatic angiosarcoma: findings on multiphasic contrast-enhanced helical CT do not mimic hepatic hemangioma. AJR Am J Roentgenol 175:165–70. https://doi.org/https://doi.org/10.2214/ajr.175.1.1750165
24. Chien C-Y, Hwang C-c, Yeh C-n, Chen H-y, Wu J-T, et al (2012) Liver angiosarcoma, a rare liver malignancy, presented with intraabdominal bleeding due to rupture-a case report. World J Surg Oncol 10:23. https://doi.org/https://doi.org/10.1186/1477-7819-10-23
25. Lee S-W, Song C-Y, Gi Y-H, Kang S-B, Kim Y-S, et al (2008) Hepatic angiosarcoma manifested as recurrent hemoperitoneum. World J Gastroenterol 14:2935–8. https://doi.org/https://doi.org/10.3748/wjg.14.2935
26. Leowardi C, Hormann Y, Hinz U, Wente MN, Hallscheidt P, et al (2006) Ruptured angiosarcoma of the liver treated by emergency catheter-directed embolization. World J Gastroenterol 12:804–8. https://doi.org/https://doi.org/10.3748/wjg.v12.i5.804
27. Mortelé KJ, Ros PR (2001) Cystic focal liver lesions in the adult: differential CT and MR imaging features. Radiographics 21:895–910. https://doi.org/https://doi.org/10.1148/radiographics.21.4.g01jl16895
28. Borhani AA, Wiant A, Heller MT (2014) Cystic hepatic lesions: a review and an algorithmic approach. AJR Am J Roentgenol 203:1192–204. https://doi.org/https://doi.org/10.2214/AJR.13.12386
29. Chen Z-Y, Qi Q-H, Dong Z-L (2002) Etiology and management of hemorrhage in spontaneous liver rupture: a report of 70 cases. World J Gastroenterol 8:1063–6. https://doi.org/https://doi.org/10.3748/wjg.v8.i6.1063
30. Kalb B, Sarmiento JM, Kooby DA, Adsay NV, Martin DR (2009) MR imaging of cystic lesions of the pancreas. Radiographics 29:1749–65. https://doi.org/https://doi.org/10.1148/rg.296095506
31. Sakaguchi T, Nakamura S, Suzuki S, Konno H, Fujita K, et al (2000) Intracystic hemorrhage of pancreatic serous cystadenoma after renal transplantation: report of a case. Surg Today 30:667–9. https://doi.org/https://doi.org/10.1007/s005950070111
32. Tokue H, Morita H, Tokue A, Tsushima Y (2017) Successful management of life-threatening bleeding of intraductal papillary mucinous neoplasms in the pancreatic head. SAGE Open Med Case Rep 5:2050313X17741014. https://doi.org/10.1177/2050313X17741014
33. Sahani DV, Kadavigere R, Saokar A, Fernandez-del Castillo C, Brugge WR, Hahn PF (2005) Cystic pancreatic lesions: a simple imaging-based classification system for guiding management. Radiographics 25:1471–84. https://doi.org/https://doi.org/10.1148/rg.256045161
34. Bilimoria KY, Tomlinson JS, Merkow RP, Stewart AK, Ko CY, et al (2007) Clinicopathologic features and treatment trends of pancreatic neuroendocrine tumors: analysis of 9,821 patients. J Gastrointest Surg 11:1460–9. https://doi.org/https://doi.org/10.1007/s11605-007-0263-3
35. Lewis RB, Lattin Jr M, Grant E, Paal E (2010) Pancreatic endocrine tumors: radiologic–clinicopathologic correlation. Radiographics 30:1445–64. https://doi.org/https://doi.org/10.1148/rg.306105523
36. Sahni VA, Mortelé KJ (2009) The bloody pancreas: MDCT and MRI features of hypervascular and hemorrhagic pancreatic conditions. AJR Am J Roentgenol 192:923–35. https://doi.org/https://doi.org/10.2214/AJR.08.1602
37. Banks PA, Bollen TL, Dervenis C, Gooszen HG, Johnson CD, et al (2013) Classification of acute pancreatitis—2012: revision of the Atlanta classification and definitions by international consensus. Gut 62:102–11. https://doi.org/https://doi.org/10.1136/gutjnl-2012-302779
38. Karaosmanoglu AD, Arslan S, Ozbay Y, Sokmensuer C, Ozogul E, Karcaaltincaba M (2020) Pancreatic Endometrioma Presenting with Spontaneous Hemorrhagic Rupture. Pancreas 49:e23–e4. https://doi.org/https://doi.org/10.1097/MPA.0000000000001510
39. Kaza R, Azar S, Al-Hawary M, Francis I (2010) Primary and secondary neoplasms of the spleen. Cancer Imaging 10:173–82. https://doi.org/https://doi.org/10.1102/1470-7330.2010.0026
40. Hahn PF, Weissleder R, Stark D, Saini S, Elizondo G, Ferrucci J (1988) MR imaging of focal splenic tumors. AJR Am J Roentgenol 150:823–7. https://doi.org/https://doi.org/10.2214/ajr.150.4.823
41. Fiorentino MD, Monteiro JMC, de Siqueira REB, Kim EIM, Curi AP, et al (2019) Primary splenic angiosarcoma: a rare entity often associated with rupture and hemoperitoneum. Autops Case Rep 9: e2019100. https://doi.org/https://doi.org/10.4322/acr.2019.100
42. Urrutia M, Mergo PJ, Ros LH, Torres GM, Ros PR (1996) Cystic masses of the spleen: radiologic-pathologic correlation. Radiographics 16:107–29. https://doi.org/https://doi.org/10.1148/radiographics.16.1.107

43. Spencer N, Arthur R, Stringer M (1996) Ruptured splenic epidermoid cyst: case report and imaging appearances. Pediatr Radiol 26:871–3. https://doi.org/https://doi.org/10.1007/BF03178039
44. Matsubayashi H, Kuraoka K, Kobayashi Y, Yokota T, Iiri T, et al (2001) Ruptured epidermoid cyst and haematoma of spleen: a diagnostic clue of high levels of serum carcinoembryonic antigen, carbohydrate antigen 19-9 and Sialyl Lewis x. Dig Liver Dis 33:595–9. https://doi.org/https://doi.org/10.1016/s1590-8658(01)80114-6
45. Sharma D (2009) Sub capsular splenectomy for delayed spontaneous splenic rupture in a case of sickle cell anemia. World J Emerg Surg 4:1–3. https://doi.org/https://doi.org/10.1186/1749-7922-4-17
46. Lopes Vendrami C, Parada Villavicencio C, DeJulio TJ, Chatterjee A, Casalino DD, et al (2017) Differentiation of solid renal tumors with multiparametric MR imaging. Radiographics 37:2026–42. https://doi.org/https://doi.org/10.1148/rg.2017170039
47. Silverman SG, Mortele KJ, Tuncali K, Jinzaki M, Cibas ES (2007) Hyperattenuating renal masses: etiologies, pathogenesis, and imaging evaluation. Radiographics 27:1131–43. https://doi.org/https://doi.org/10.1148/rg.274065147
48. Rosenkrantz AB, Hindman N, Fitzgerald EF, Niver BE, Melamed J, Babb JS (2010) MRI features of renal oncocytoma and chromophobe renal cell carcinoma. AJR Am J Roentgenol 195:W421–W7. https://doi.org/https://doi.org/10.2214/AJR.10.4718
49. Prando A, Prando D, Prando P (2006) Renal cell carcinoma: unusual imaging manifestations. Radiographics 26:233–44. https://doi.org/https://doi.org/10.1148/rg.261055060
50. Yamakado K, Tanaka N, Nakagawa T, Kobayashi S, Yanagawa M, Takeda K (2002) Renal angiomyolipoma: relationships between tumor size, aneurysm formation, and rupture. Radiology 225:78–82. https://doi.org/https://doi.org/10.1148/radiol.2251011477
51. Wood III CG, Stromberg III LJ, Harmath CB, Horowitz JM, Feng C, et al (2015) CT and MR imaging for evaluation of cystic renal lesions and diseases. Radiographics 35:125–41. https://doi.org/https://doi.org/10.1148/rg.351130016
52. Agnello F, Albano D, Micci G, Di Buono G, Agrusa A, et al (2020) CT and MR imaging of cystic renal lesions. Insights Imaging 11:1–11. https://doi.org/https://doi.org/10.1186/s13244-019-0826-3
53. Antopol W, Goldman L (1948) Subepithelial hemorrhage of renal pelvis simulating neoplasm. Urol Cutaneous Rev 52:189–95
54. Gayer G, Desser TS, Hertz M, Osadchy A, Daniel BL, Zissin R (2011) Spontaneous suburothelial hemorrhage in coagulopathic patients: CT diagnosis. AJR Am J Roentgenol 197:W887–W90. https://doi.org/https://doi.org/10.2214/AJR.11.6474
55. Kim JW, Kim JY, Ahn ST, Park TY, Oh MM, et al (2019) Spontaneous perirenal hemorrhage (Wunderlich syndrome): An analysis of 28 cases. Am J Emerg Med 37:45–7. https://doi.org/https://doi.org/10.1016/j.ajem.2018.04.045
56. Chao C-T, Wang W-J, Ting J-T (2013) Wünderlich syndrome from lupus-associated vasculitis. Am J Kidney Dis 61:167–70. https://doi.org/https://doi.org/10.1053/j.ajkd.2012.06.027
57. Wong-You–Cheong JJ, Woodward PJ, Manning MA, Sesterhenn IA (2006) Neoplasms of the urinary bladder: radiologic–pathologic correlation. Radiographics 26:553–80. https://doi.org/https://doi.org/10.1148/rg.262055172
58. Raman SP, Fishman EK (2014) Bladder malignancies on CT: the underrated role of CT in diagnosis. AJR Am J Roentgenol 203:347–54. https://doi.org/https://doi.org/10.2214/AJR.13.12021
59. Johnson PT, Horton KM, Fishman EK (2009) Adrenal mass imaging with multidetector CT: pathologic conditions, pearls, and pitfalls. Radiographics 29:1333–51. https://doi.org/https://doi.org/10.1148/rg.295095027
60. Karaosmanoglu AD, Uysal A, Arslan S, Sokmensuer C, Leblebici C, et al (2021) Can we differentiate neoplastic and non-neoplastic spontaneous adrenal bleeding? Imaging findings with radiopathologic correlation. Abdom Radiol (NY) 46:1091–1102. https://doi.org/https://doi.org/10.1007/s00261-020-02750-w
61. Rao RH, Vagnucci AH, Amico JA (1989) Bilateral massive adrenal hemorrhage: early recognition and treatment. Ann Intern Med 110:227–35. https://doi.org/https://doi.org/10.7326/0003-4819-110-3-227
62. Wells ML, Hansel SL, Bruining DH, Fletcher JG, Froemming AT, et al (2018) CT for evaluation of acute gastrointestinal bleeding. Radiographics 38:1089–107. https://doi.org/https://doi.org/10.1148/rg.2018170138
63. Huprich JE, Barlow JM, Hansel SL, Alexander JA, Fidler JL (2013) Multiphase CT enterography evaluation of small-bowel vascular lesions. AJR Am J Roentgenol 201:65–72. https://doi.org/https://doi.org/10.2214/AJR.12.10414
64. Abbas MA, Collins JM, Olden KW (2002) Spontaneous intramural small-bowel hematoma: imaging findings and outcome. AJR Am J Roentgenol 179:1389–94. https://doi.org/https://doi.org/10.2214/ajr.179.6.1791389
65. Molina-Barea R, Pérez-Cabrera B, Hernández-García MD, Navarro-Freire F, Jiménez-Ríos JA (2015) Acute abdomen due to complicated intramural duodenal haematoma. Case report and literature review. Cir Cir 83:146–50. https://doi.org/https://doi.org/10.1016/j.circir.2015.04.011
66. Rizzo S, Calareso G, De Maria F, Zanagnolo V, Lazzari R, et al (2013) Gynecologic tumors: how to communicate imaging results to the surgeon. Cancer Imaging 13:611. https://doi.org/https://doi.org/10.1102/1470-7330.2013.0054
67. Lin EP, Bhatt S, Dogra VS (2008) Diagnostic clues to ectopic pregnancy. Radiographics 28:1661–71. https://doi.org/https://doi.org/10.1148/rg.286085506
68. Lee YR (2011) CT imaging findings of ruptured ovarian endometriotic cysts: emphasis on the differential diagnosis with ruptured ovarian functional cysts. Korean J Radiol 12:59–65. https://doi.org/https://doi.org/10.3348/kjr.2011.12.1.59
69. Mota MMdS, Bezerra ROF, Garcia MRT (2018) Practical approach to primary retroperitoneal masses in adults. Radiol Bras 51:391–400. https://doi.org/https://doi.org/10.1590/0100-3984.2017.0179
70. Rajiah P, Sinha R, Cuevas C, Dubinsky TJ, Bush Jr WH, Kolokythas O (2011) Imaging of uncommon retroperitoneal masses. Radiographics 31:949–76. https://doi.org/https://doi.org/10.1148/rg.314095132
71. Vos CG, Hoksbergen AW (2011) Fatal retroperitoneal bleeding caused by metastasis of a sigmoid carcinoma. Case Rep Med 2011:373047. https://doi.org/https://doi.org/10.1155/2011/373047
72. Della Vecchia J, Blazar E (2020) A Missed Celiac Artery Aneurysm Leading to Rupture: A Case Report. Clin Pract Cases Emerg Med 4:440–42. https://doi.org/https://doi.org/10.5811/cpcem.2020.6.46513
73. Harris K, Chalhoub M, Koirala A (2010) Gastroduodenal artery aneurysm rupture in hospitalized patients: an overlooked diagnosis. World J Gastrointest Surg 2:291–4. https://doi.org/https://doi.org/10.4240/wjgs.v2.i9.291
74. Chernyak V, Fowler KJ, Kamaya A, Kielar AZ, Elsayes KM, et al (2018) Liver Imaging Reporting and Data System (LI-RADS) Version 2018: Imaging of Hepatocellular Carcinoma in At-Risk Patients. Radiology 289:816–830. https://doi.org/https://doi.org/10.1148/radiol.2018181494